EUROPEAN ORGANIZATION FOR NUCLEAR RESEARCH
European Laboratory for Particle Physics

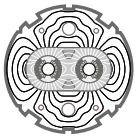

Large Hadron Collider Project **LHC Project Report 602**

Determination of Chromaticity by the Measurement of Head-Tail Phase Shifts: simulations, results from the SPS and a robustness study for the LHC

S. Fartoukh (SL/AP) and R. Jones (SL/BI)

Abstract

The feasibility of chromaticity determination by measuring head-tail phase shifts has been shown both in the CERN-SPS and at HERA (DESY). These measurements, although verifying the technique, also raised some questions concerning its use for everyday operation. This report includes the source of the missing constant factor that was found between theory and experiment, the consequences of the RF bucket deformation due to the acceleration in the SPS and detailed simulations and calculations on the LHC to estimate the accuracy of the head-tail chromaticity technique in the presence of other possible perturbations such as non-linear chromaticity, coupling and transverse impedance.

Administrative Secretariat
LHC Division
CERN
CH-1211 Geneva 23
Switzerland

Geneva, 29 July 2002

1 Introduction

The tight tolerances on beam parameters required for successful LHC operation implies a good knowledge of the chromaticity throughout the cycle. However, many of the methods currently used to measure chromaticity in circular machines (see [1] and references therein) are likely to be incompatible with LHC high intensity running. For example, the most common method, of measuring the betatron tune as a function of beam energy, might be difficult to implement due to the tight tolerances imposed on the betatron tune, and on the beam energy variations the LHC will accept. Chromaticity can also be calculated from the amplitude of the synchrotron sidebands observed in the transverse frequency spectrum. However, this method suffers from resonant behaviour not linked to chromaticity and the fact that the low synchrotron tune of the LHC would make it difficult to distinguish these sidebands from the main betatron tune peak. The width of the betatron tune peak itself, or the phase response of the beam transfer function also gives a measure of chromaticity, but requires a knowledge of how the momentum spread in the beam will changes during the ramp of the LHC.

The determination of chromaticity by following the evolution of head-tail phase shifts after a transverse dipole excitation is a technique which does not rely on an accurate knowledge of the fractional part of the betatron tune and, for a machine operating well above transition, is virtually independent of beam energy. Early experiments in the CERN-SPS [2] and at HERA-p (DESY) [3] have shown the feasibility of the technique for high-energy proton beams. More recent experiments [4] have highlighted several questions concerning the use of this technique for accurate chromaticity determination. The most important of these concerned a constant factor that appeared between the calculation of chromaticity via traditional techniques and that which was calculated from head-tail phase shift measurements.

This paper compares the results of tracking studies with the simple two-particle model on which the original head-tail theory was based in an attempt to explain the missing constant factor (Section 2). The outcome of these results indirectly led to the source of the missing factor, which was ultimately found to lie with the experimental method rather than the theory, and is explained in detail (Section 3). This being said, theory and experiment will be compared in Section 4 to analyse in particular the consequences of the RF bucket deformation due to the acceleration in the SPS. Finally, detailed simulations performed for the LHC will be presented in Sections 5 and 6 to study the robustness of the head-tail chromaticity measurement technique in the presence of other possible sources of perturbation such as non-linear chromaticity (Q'' and Q'''), linear betatron coupling and transverse impedance.

2 The Head-Tail Principle and its simulation

In Ref. [2], a two-particle model was used to give an analytical estimate of the evolution of the betatron phase shift between the head and the tail of a kicked beam due to a non-zero chromaticity. Neglecting the non-linearity of the synchrotron motion, this result can be easily extended to the case of an arbitrary longitudinal bunch distribution (Sub-section 2.1). To deal with the general case, a multi-particle tracking program was written in order to depict correctly the synchrotron motion (with or without acceleration) and to include other perturbations such as dispersion, off-momentum beta-beating and non-linear chromaticity (as Q'' or Q'''). After a detailed description of this program (Paragraph 2.2.1), tracking results and analytical estimates are compared in the case of a stationary bucket and a purely linear chromaticity (Paragraph 2.2.2). The case of an accelerating bucket will be treated in detail in Section 4, and the influence of the non-linear chromaticity studied in Section 5.

2.1 Multi-particle dynamics and an analytical estimate in the linear optics approximation

Assuming longitudinal stability and neglecting the non-linearities of the synchrotron motion, a single particle will rotate in longitudinal phase space at a frequency equal to the synchrotron frequency:

$$\left\{ \begin{array}{rcl} z(s;r,\phi_s) & = & r\,\cos\left(2\pi Q_s\,s/C+\phi_s\right) \\ \delta(s;r,\phi_s) & = & -\dfrac{2\pi Q_s}{\eta\,C}\,r\,\sin\left(2\pi Q_s\,s/C+\phi_s\right). \end{array} \right. \tag{1}$$

Here C is the ring circumference, s the curvilinear abscissa around the ring, Q_s the synchrotron tune and $\eta = 1/\gamma^2 - \alpha^2$ the slippage factor (with α the momentum compaction); z denotes the relative longitudinal coordinate within the bunch defined by $z = 0$ for the synchronous particle and $z > 0$ at the bunch head, δ is the relative momentum deviation. The quantities r and ϕ_s parametrise the initial conditions of the particle considered.
After a transverse kick the particle also undergoes transverse motion which, turn after turn, can be described by

$$y(n;r,\phi_s) = A\sin\left(2n\pi Q + \theta(n;r,\phi_s)\right)\,, \tag{2}$$

with A a constant, n the turn number after the kick, Q the betatron tune and $\theta(n;r,\phi_s)$ a phase shift which, assuming a purely linear chromaticity (i.e. $Q'' = Q''' = \ldots = 0$), is given by

$$\theta(n;r,\phi_s) = \frac{2\pi}{C}\int_0^{nC} ds\,Q'\times\delta(s;r,\phi_s) = \frac{2\pi\,Q'}{\eta\,C}\left(\underbrace{r\,\cos\left(2n\pi Q_s+\phi_s\right)}_{=\,z(nC;r,\phi_s)} - \underbrace{r\,\cos\left(\phi_s\right)}_{=\,z(0;r,\phi_s)}\right)\,. \tag{3}$$

This phase-shift can then be expressed as a function of the actual position $\left(\tau \stackrel{\text{def}}{=} z/c\,,\,\delta\right)$ of the particle in longitudinal phase space. Indeed, using Eq. (1), we have

$$r\,\cos\left(\phi_s\right) = r\,\cos\left(2n\pi Q_s+\phi_s-2n\pi Q_s\right) = z\,\cos\left(2n\pi Q_s\right) - \frac{\eta\,C}{2\pi Q_s}\,\delta\,\sin\left(2n\pi Q_s\right), \tag{4}$$

leading to

$$\theta(n;r,\phi_s)\equiv\theta(n;\tau,\delta) = \frac{\omega_0\,Q'}{\eta}\left(1-\cos(2n\pi Q_s)\right)\times\tau + \frac{Q'}{Q_s}\sin(2n\pi Q_s)\times\delta\,, \tag{5}$$

with $\omega_0 = 2\pi c/C$ the angular revolution frequency. Finally, by combining this relation with Eq. (2), one gets

$$\begin{aligned} y\left(n;r,\phi_s\right)\equiv y(n;\tau,\delta) &= A\,\sin\Big[2n\pi Q + \frac{\omega_0\,Q'}{\eta}\,\tau\,\left(1-\cos(2n\pi Q_s)\right) + \frac{Q'}{Q_s}\,\delta\,\sin(2n\pi Q_s)\Big] \\ &= A\,\cos\left(Q'/Q_s\,\delta\,\sin(2n\pi Q_s)\right)\,\sin\Big[2n\pi Q + \frac{\omega_0\,Q'}{\eta}\,\tau\,\left(1-\cos(2n\pi Q_s)\right)\Big] + \\ &\quad A\,\sin\left(Q'/Q_s\,\delta\,\sin(2n\pi Q_s)\right)\,\cos\Big[2n\pi Q + \frac{\omega_0\,Q'}{\eta}\,\tau\,\left(1-\cos(2n\pi Q_s)\right)\Big]\,. \end{aligned} \tag{6}$$

At turn n, the transverse excursion $\langle y \rangle (\hat{\tau}; n)$ of the slice $\hat{z} \stackrel{\text{def}}{=} c\hat{\tau}$ can then be easily obtained by multiplying the previous relation by the actual longitudinal distribution $\rho(\hat{\tau}, \delta; n)$ of the bunch, integrating over δ and normalising the result obtained in the following way:

$$\langle y \rangle (\hat{\tau}; n) = A (\hat{\tau}; n) \, \sin (2n\pi Q + \phi_\beta (\hat{\tau}; n)) + B (\hat{\tau}; n) \, \cos (2n\pi Q + \phi_\beta (\hat{\tau}; n))$$

$$\text{with} \left\{ \begin{array}{rcl} A (\hat{\tau}; n) & = & A \displaystyle\int d\delta \, \rho (\hat{\tau}, \delta; n) \, \cos (Q'/Q_s \, \delta \, \sin(2n\pi Q_s)) \; / \; \int d\delta \, \rho (\hat{\tau}, \delta; n) \\ B (\hat{\tau}; n) & = & A \displaystyle\int d\delta \, \rho (\hat{\tau}, \delta; n) \, \sin (Q'/Q_s \, \delta \, \sin(2n\pi Q_s)) \; / \; \int d\delta \, \rho (\hat{\tau}, \delta; n) \\ \phi_\beta (\hat{\tau}; n) & = & \dfrac{\omega_0 Q'}{\eta} \, \hat{\tau} \, (1 - \cos(2n\pi Q_s)) \, . \end{array} \right. \tag{7}$$

After the RF capture, the distribution $\rho (\tau, \delta; n)$ becomes independent of n (assuming no coherent longitudinal oscillation) and is an even function of δ. As a result, the cosine-amplitude occurring in Eq. (7) (coefficient B) vanishes.

Concerning the head-tail phase shift, Eq. (7) reproduces exactly the analytical estimate derived in Ref. [2] and obtained with a simple two-particle model. If we consider the evolution of two longitudinal positions within a single bunch separated in time by $\Delta\tau$, then the phase difference in the transverse oscillation of these two slices is given by

$$\Delta\phi_\beta(\Delta\tau; n) = \frac{\omega_0 \, Q'}{\eta} \, \Delta\tau \, (1 - \cos(2n\pi Q_s)) \, . \tag{8}$$

This phase difference is a maximum when $nQ_s = 1/2$ (i.e. after half a synchrotron period) and is directly related to the chromaticity:

$$\Delta\phi_\beta^{\max}(\Delta\tau) = 2 \, \Delta\tau \, \frac{\omega_0 \, Q'}{\eta} \;\; \text{or} \;\; Q' = \frac{\eta \, \Delta\phi_\beta^{\max}(\Delta\tau)}{2 \, \omega_0 \, \Delta\tau} \, . \tag{9}$$

On the other hand, Eq. (7) contains additional information related to the decoherence of the signal observed. For instance, for a Gaussian bunch, the distribution $\rho(\tau, \delta)$ is given by

$$\rho(\tau, \delta) = \frac{1}{2\pi \, \sigma_\tau \, \sigma_\delta} \, \exp\left(-\frac{\tau^2}{2\sigma_\tau^2}\right) \, \exp\left(-\frac{\delta^2}{2\sigma_\delta^2}\right) \;\; \text{with} \;\; \sigma_\delta = \frac{\omega_0 \, Q_s}{|\eta|} \, \sigma_\tau \, , \tag{10}$$

and the sine-amplitude $A (\hat{\tau}; n)$ occurring in Eq. (7) is given by

$$A (\hat{\tau}; n) = A \, \exp\left[- \left(\frac{\omega_0 \, Q'}{\eta} \, \sigma_\tau \, \sin(2n\pi Q_s) \right)^2 / 2 \right] \, , \tag{11}$$

which is independent of $\hat{\tau}$ in this particular case. Therefore, in the presence of a non-zero chromaticity, the signal envelope decoheres and recoheres every half synchrotron period.

2.2 Influence of synchrotron non-linearities

Including the non-linearities of the RF potential in our analytical treatment would require the use of elliptic functions, which has been found extremely difficult, if not impossible in the case of an accelerating bucket. Therefore a beam simulator has been written where the interactions between the beam and the head-tail monitor is correctly depicted at just the right level of complexity, i.e. containing an exact description of the synchrotron motion and including all the possible chromatic aberrations in the one-turn transverse map. The main features of this simulator are described below. The results obtained in the case of a stationary SPS bucket and a purely linear chromaticity are shown in paragraph 2.2.2 and compared to the analytical estimate given in Eq. (8).

Parameter	Symbol	Units	Value	
Ring Circumference	C	m	6906.765	
Harmonic number	h	[1]	4620 $(200\,\mathrm{MHz})$	
Momentum compaction	α	$[10^{-3}]$	1.8539	
Energy	E_s	[GeV]	265.000	303.910
Relativistic factor	γ	[1]	282.434	323.904
Slippage factor	η	$[10^{-3}]$	-1.8413	-1.8443
Peak RF Voltage	V_{RF}	[MV]	4.021	3.869
Synchronous RF phase	ϕ_s	$[^\circ]$	26.60	27.72
Synchronous RF voltage	$V_{\mathrm{RF}}\sin(\phi_s)$	[MV]	1.8	1.8
Synchrotron tune (at zero synchrotron amplitude)	Q_s	[turns]	233	256
Bucket half-height	$\delta_{\max}$	$[10^{-3}]$	0.67	0.60
Bucket head w.r.t. ϕ_s	$\tau_{\max}$	[ns]	1.76	1.73
Bucket tail w.r.t. ϕ_s	$\tau_{\min}$	[ns]	-1.03	-1.00

Table 1: Parameters relevant to the SPS RF system, RF voltage, synchronous phase and bucket description for 2 different energies (voltage programme in Spring 2001, courtesy of L. Normann).

2.2.1 Description of tracking parameters

One-turn map.

In the four dimensional phase space (y, y', z, δ), the one-turn map is obtained via the concatenation of the two following transformations:

a) the transport across the RF system described by

$$\mathcal{Y} \stackrel{\mathrm{def}}{=} \begin{pmatrix} y \\ y' \\ z = c\Delta t \\ \delta = \Delta E/E_{s_i} \end{pmatrix} \rightsquigarrow \begin{pmatrix} y \\ E_{s_i}/E_{s_f}\, y' \\ z \\ E_{s_i}/E_{s_f}\, \delta + eV_{\mathrm{RF}}/E_{s_f}\, [\sin(\phi_s + 2\pi h z/C) - \sin(\phi_s)] \end{pmatrix} . \tag{12}$$

Here e denotes the electric charge of the particle, h is the harmonic number, C the ring circumference, V_{RF} the peak RF voltage, E_{s_i} and $E_{s_f} \equiv E_{s_i} + eV_{\mathrm{RF}}\sin(\phi_s)$ the initial and final energy of the synchronous particle with $V_{\mathrm{RF}}\sin(\phi_s)$ representing the synchronous accelerating voltage. Note that with the convention chosen for the z coordinate, $z > 0$ at the bunch head, the stability of the synchrotron motion implies $|\phi_s| < \pi/2$. The basic parameters relevant to the SPS RF system are listed in Table 1 at the energies of 265 GeV and 303.91 GeV, where most of the beam measurements were performed.

b) the transport around the ring described by the following δ-dependent 4×4 symplectic $R-$matrix:

$$R(\delta) = \begin{pmatrix} R_{11} & R_{12} & 0 & R_{16} \\ R_{21} & R_{22} & 0 & R_{26} \\ R_{51} & R_{52} & 1 & R_{56} \\ 0 & 0 & 0 & 1 \end{pmatrix} , \tag{13}$$

$$\text{with} \quad \begin{cases} R_{11} = \cos(2\pi Q_x) + \alpha_x \, \sin(2\pi Q_x) \\ R_{12} = \beta_x \sin(2\pi Q_x) \\ R_{21} = -\gamma_x \sin(2\pi Q_x) \\ R_{22} = \cos(2\pi Q_x) - \alpha_x \, \sin(2\pi Q_x) \end{cases}, \begin{cases} R_{16} = \quad D_x \, (1 - R_{11}) - D'_x R_{12} \\ R_{26} = \quad D'_x \, (1 - R_{22}) - D_x R_{21} \\ R_{51} = \quad D'_x \, (1 - R_{11}) + D_x R_{21} \\ R_{52} = -D_x \, (1 - R_{22}) - D'_x R_{12} \\ R_{56} = \; \eta \, C - D_x \, R_{51} - D'_x \, R_{52} \end{cases}, \tag{14}$$

$$\text{and} \quad \begin{cases} \beta_x(\delta) \; = \beta_x^{(0)} + \beta_x^{(1)} \delta + \ldots \\ \alpha_x(\delta) = \alpha_x^{(0)} + \alpha_x^{(1)} \delta + \ldots \\ \gamma_x(\delta) \; = (1 + \alpha_x^2)/\beta_x \\ Q_x(\delta) = Q_x + Q'_x \delta + Q''_x \delta^2 + \ldots \, . \end{cases}$$

Here η represents the slippage factor, $\alpha_x, \beta_x, \gamma_x, D_x \, D'_x$ the horizontal or vertical Twiss parameters, dispersion and angular dispersion at the location of the RF cavity, and Q_x is the betatron tune. Assuming reasonable transverse kicks of the order of one r.m.s. beam size σ, an off-momentum beta-beating as large as 20% over the bunch energy distribution (i.e. twice more than is expected for the squeezed optics of the LHC [5, p. 4]) and a dispersion function going from a few centimetres up to 1 m, the perturbation induced on the head-tail phase shift is almost invisible in the simulations. This aspect will therefore be omitted in all the rest of the paper. The discussion concerning the contribution of the non-linear chromaticity Q'' and/or Q''' will be treated in Section 5.

Invariant of the synchrotron motion.
For an appropriate choice of initial distribution for the bunch in longitudinal phase-space, we start by extracting a prime integral for the synchrotron motion from the transformations (12) and (13). Under the approximation of an adiabatic acceleration, i.e. $eV_{\rm RF} \sin(\phi_s)/E_s \ll 1$ and neglecting the synchro-betatron coupling due to the dispersion, the change of synchrotron coordinates from turn to turn is given by

$$\begin{cases} \Delta z \;\; \approx \;\; C \, \dfrac{dz}{ds} \;\; = \;\; \eta \, C \, \delta \\ \Delta \delta \;\; \approx \;\; C \, \dfrac{d\delta}{ds} \;\; = \;\; \dfrac{eV_{\rm RF}}{E_s} \left(\sin(\phi_s + 2\pi h z/C) - \sin(\phi_s) \right) \end{cases} \tag{15}$$

As a result, the quantity

$$g(z, \delta) \stackrel{\rm def}{=} \left(\frac{\delta}{\delta_{\max}} \right)^2 + \frac{V(2\pi h z/C)}{V(\pi - 2\phi_s)} \tag{16}$$

is a constant of motion (normalised Hamiltonian), with

$$V(\phi) \stackrel{\rm def}{=} \frac{1}{2} \left(\cos(\phi_s) - \cos(\phi + \phi_s) - \phi \, \sin(\phi_s) \right) \;\; \text{and} \;\; \delta_{\max} = \sqrt{\frac{2eV_{RF}}{\pi h E_s \, |\eta|} \, V(\pi - 2\phi_s)} \tag{17}$$

the bucket half-height; the condition for RF capture is then given by

$$g(z, \delta) \leq 1 \; . \tag{18}$$

Initial distribution in longitudinal phase space.
In order to warrant the turn-by-turn conservation of the distribution $\rho(z, \delta)$, the latter must be a function of g and thus conforms to the contours of the normalised Hamiltonian (16) inside the bucket. A set of possible stationary beam distributions is obtained by writing

$$\rho(z, \delta) \propto \Theta\big[q_p^2 - g(z, \delta)\big] \times \big[q_p^2 - g(z, \delta)\big]^{\mu} , \tag{19}$$

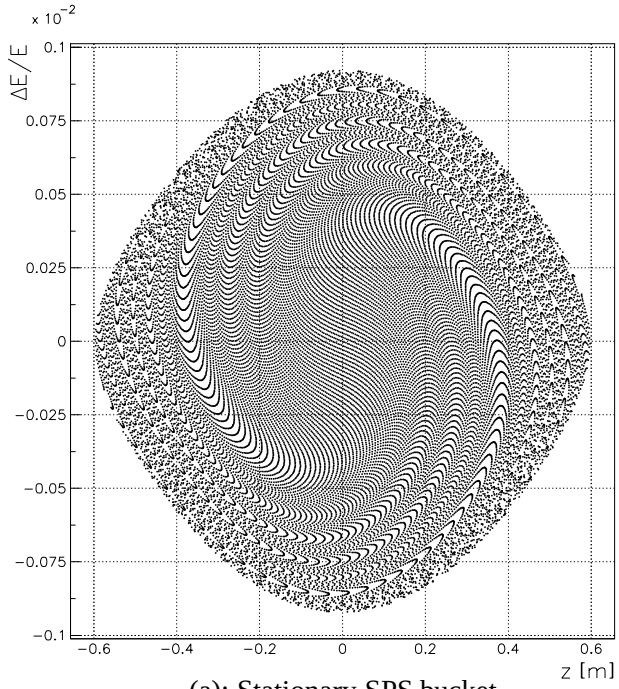

(a): Stationary SPS bucket at 303.91 GeV ($V_{\mathrm{RF}} = 3.87$ MV, $\phi_s = 0$)

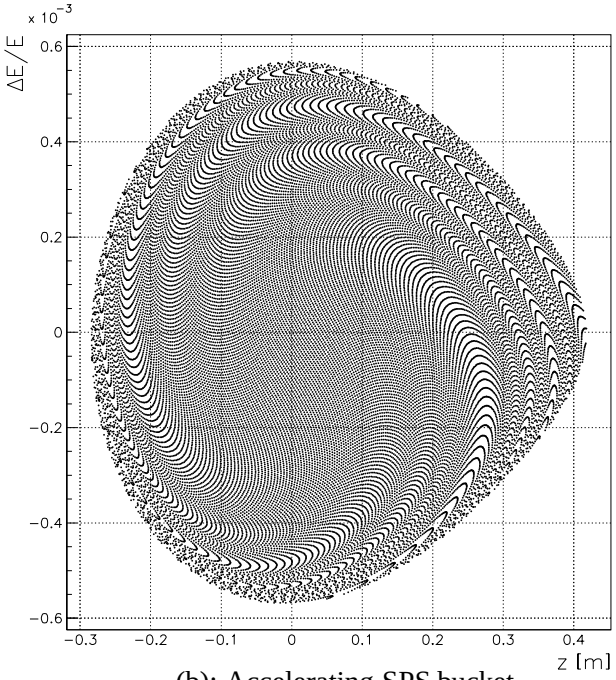

(b): Accelerating SPS bucket at 303.91 GeV ($V_{\mathrm{RF}} = 3.87$ MV, $\phi_s = 27.7°$)

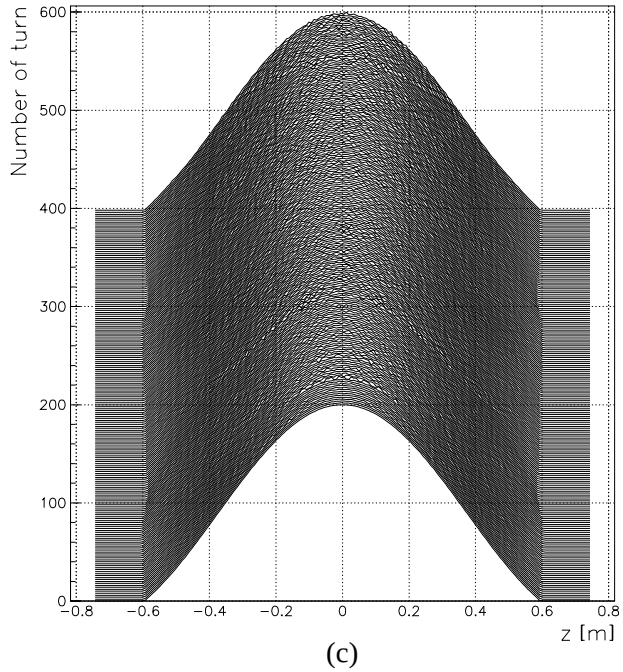

(c)

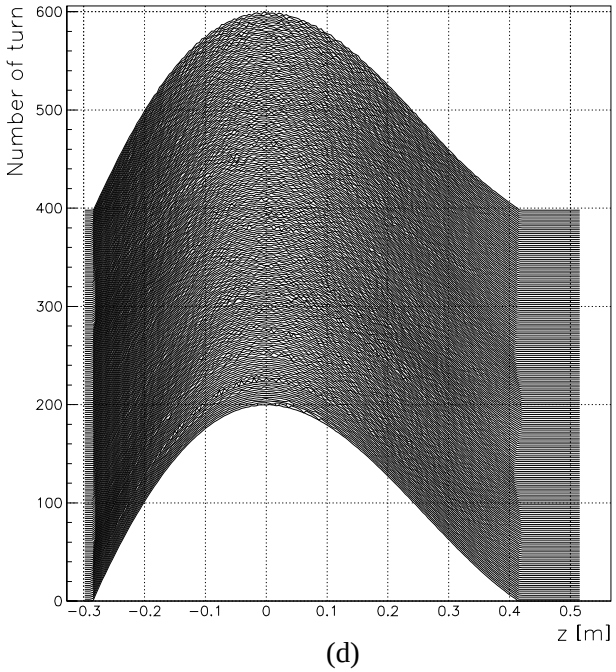

(d)

Figure 1: Longitudinal phase space of a stationary and accelerating SPS bucket at 303.91 GeV (Fig. (a) and (b)) and corresponding bunch charge distribution (Fig. (c) and (d)) tracked over 400 turns, assuming a bucket filling factor q_p of 95% and $\mu = 0.5$ in Eq. (19).

with $0 < q_p \leq 1$ the filling factor in momentum of the bucket, Θ the Heaviside step function and $\mu > -1$ an adjustable parameter quantifying the sharpness of the distribution. As an example, for $\phi_s = 0$ (no acceleration), $q_p = 1$ (100% of the bucket filled) and $\mu = 1/2$, the corresponding longitudinal distribution $\rho(z)$ is the so-called "cosine-squared" or "quasi-parabolic" distribution:

$$g(z,\delta) = \left(\frac{\delta}{\delta_{\max}}\right)^2 + \sin^2\left(\frac{\pi h z}{C}\right) \Rightarrow \rho(z) \equiv \frac{\int d\delta\ \rho(z,\delta)}{\iint d\delta\, dz\ \rho(z,\delta)} = \frac{2h}{C}\ \cos^2\left(\frac{\pi h z}{C}\right) \text{ for } |z| \leq \frac{C}{2h}\,, \tag{20}$$

which is similar to a parabolic-like distribution but has the advantage that the derivatives at the bucket edge are continuous.
After simulation for the SPS assuming a filling factor of 95% [6], the results obtained are, to a large extent, independent of the parameter μ (for μ between zero and one). In all the rest of the paper, we will therefore assume $q_p = 0.95$ and $\mu = 1/2$, that is

$$\rho(z,\delta) \propto \Theta\left[0.95^2 - g(z,\delta)\right]\ \sqrt{(0.95^2 - g(z,\delta)}\,, \tag{21}$$

with $g(z,\delta)$ given in Eq. (16). The corresponding bunch charge distribution (obtained by tracking) is shown turn after turn in Fig. 1 both for a stationary and an accelerating SPS bucket at the energy of 303.91 GeV ($V_{\rm RF}$ and ϕ_s given in Table 1).
Tracking procedure and post-processing.
At turn $n = 0$, the longitudinal plan is uniformly criss-crossed by macro-particles (typically from 5×10^5 to 10^6 particles to avoid statistical fluctuation effects) with initial conditions (z_0, δ_0) satisfying Eq. (18), and $(x_0 = 0, x'_0 = A)$ where A is the amplitude of the applied kick. Each particle is initially labelled with a weight proportional to the distribution $\rho(z,\delta)$ given in Eq. (21), then tracked using the 4D one-turn map previously described. At each turn n, the bunch is split longitudinally into a fixed number of slices (typically from 100 to 200 slices) and the average transverse position $y(\tau; n)$ of each slice is computed (with τ the time delay with respect to the central slice $\tau = 0$). The results obtained are then post-processed using Hilbert transform techniques (see e.g. [7]) to obtain both the betatron tune Q, the signal envelopes $A(\tau; n)$ and the betatron phase shifts $\phi_\beta(\tau; n)$ defining the transverse motion of each considered slice:

$$\langle y \rangle\,(\tau; n) = A(\tau; n)\ \sin\left(2n\pi Q + \phi_\beta(\tau; n)\right)\ . \tag{22}$$

2.2.2 Results of multi-particle tracking simulations for a stationary bucket

The results obtained for a stationary SPS bucket at 265 GeV are shown in Fig. 2, assuming a purely linear chromaticity Q' of 5.1 units (i.e. $\xi = Q'/Q = 0.192$ in SPS units). Here we have considered two slices of charge located at the bunch head and corresponding to $\tau = 0.5$ ns and $\tau = 1.0$ ns. The betatron phase shift is given with respect to the betatron phase measured at the bunch centre (slice $\tau = 0$).
Contrary to the simplified case treated in Sub-section 2.1 (see Eq. (11)), the signal envelope does not recohere completely after each synchrotron half-period (see Fig.'s 2(c) and 2(d)).
For the slice $\tau = 0.5$ ns, the head-tail phase shift obtained by simulation fits almost perfectly over the first synchrotron half-period ($\sim 110-120$ turns) with the analytical estimate derived in Sub-section 2.1 (see Eq. (8)). On the other hand, the perturbation induced by the non-linearity of the synchrotron motion is more significant when observing the slice $\tau = 1.0$ ns. However, in both cases, the main effect is a reduced modulation frequency for the head-tail phase shift (Q_s goes to zero for particles with large synchrotron amplitudes); within a few percent, the

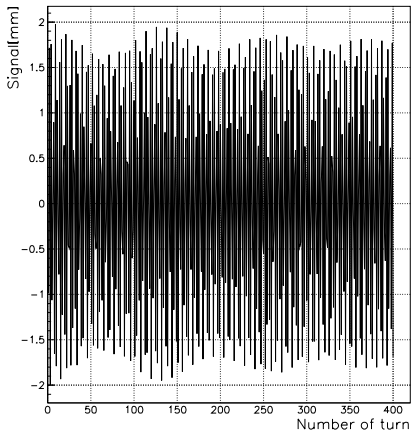

(a): Signal observed at $\tau = 0.5$ ns w.r.t. the bunch centre

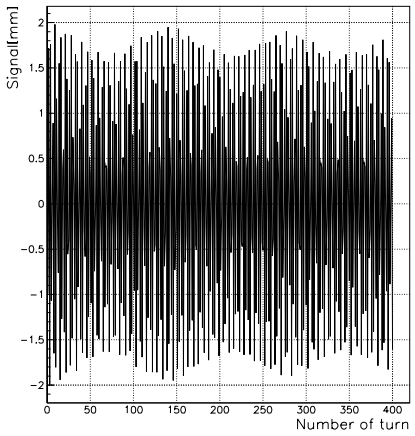

(b): Signal observed at $\tau = 1.0$ ns w.r.t. the bunch centre

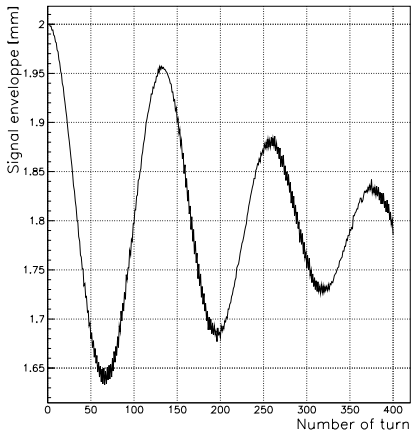

(c): Signal envelope [mm]

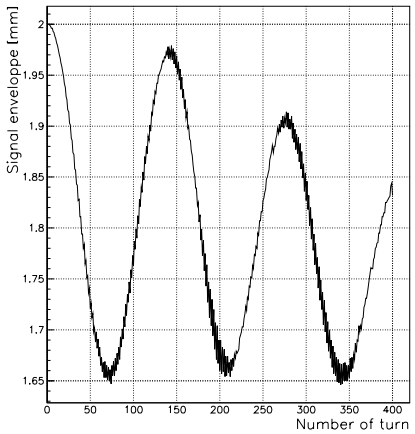

(d): Signal envelope [mm]

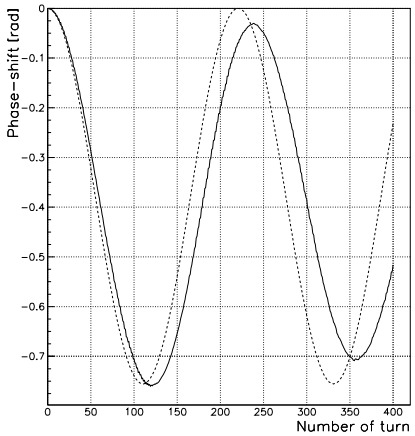

(e): Betatron phase-shift [rad]

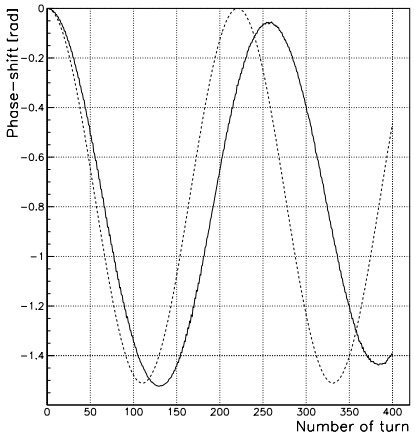

(f): Betatron phase-shift [rad]

Figure 2: SPS stationary bucket at 265 GeV. Linear chromaticity of 5.1 units. Tracking over 400 turns following the kick: signal $\langle y \rangle (\tau; n)$ (see Eq. (22)) as a function of n observed at the bunch head with a time delay of $\tau = 0.5$ ns and $\tau = 1$ ns with respect to the bunch centre (Fig.'s (a) and (b)), corresponding signal envelope $A(\tau; n)$ (Fig.'s (c) and (d)) and betatron phase-shifts $\phi_\beta(\tau; n)$ (Fig.'s (e) and (f)), and comparison with the analytical estimate given in Eq. (8) (dashed curve).

peak value $\phi_\beta^{\max}$ attained after the first synchrotron half-period is never affected. A qualitative explanation of this result will be given in Sub-section 4.2 when dealing with the case of an accelerating bucket.

The perturbations induced by the non-linearities of the synchrotron motion are even more evident in Fig. 3, where the head-tail phase shift due to Q' is shown as a function of τ for the first 341 turns after the kick. The dependence on τ of the function $\phi_\beta^{\max}(\tau)$ is clearly linear; therefore Eq. (9) can be applied "blindly" for a very accurate estimate of Q' in the following 2 cases: either one of the two slices chosen for the measurement corresponds to the centre of the bucket, or the two slices which are used are symmetrically positioned with respect to the bucket centre. On the other hand, in the case of an accelerating bucket, only the second option can be retained, the first one leading to an over or under-estimate of Q' (by 10-20%) depending on whether the measurement is made at the tail or head of the bunch respectively (see Section 4).

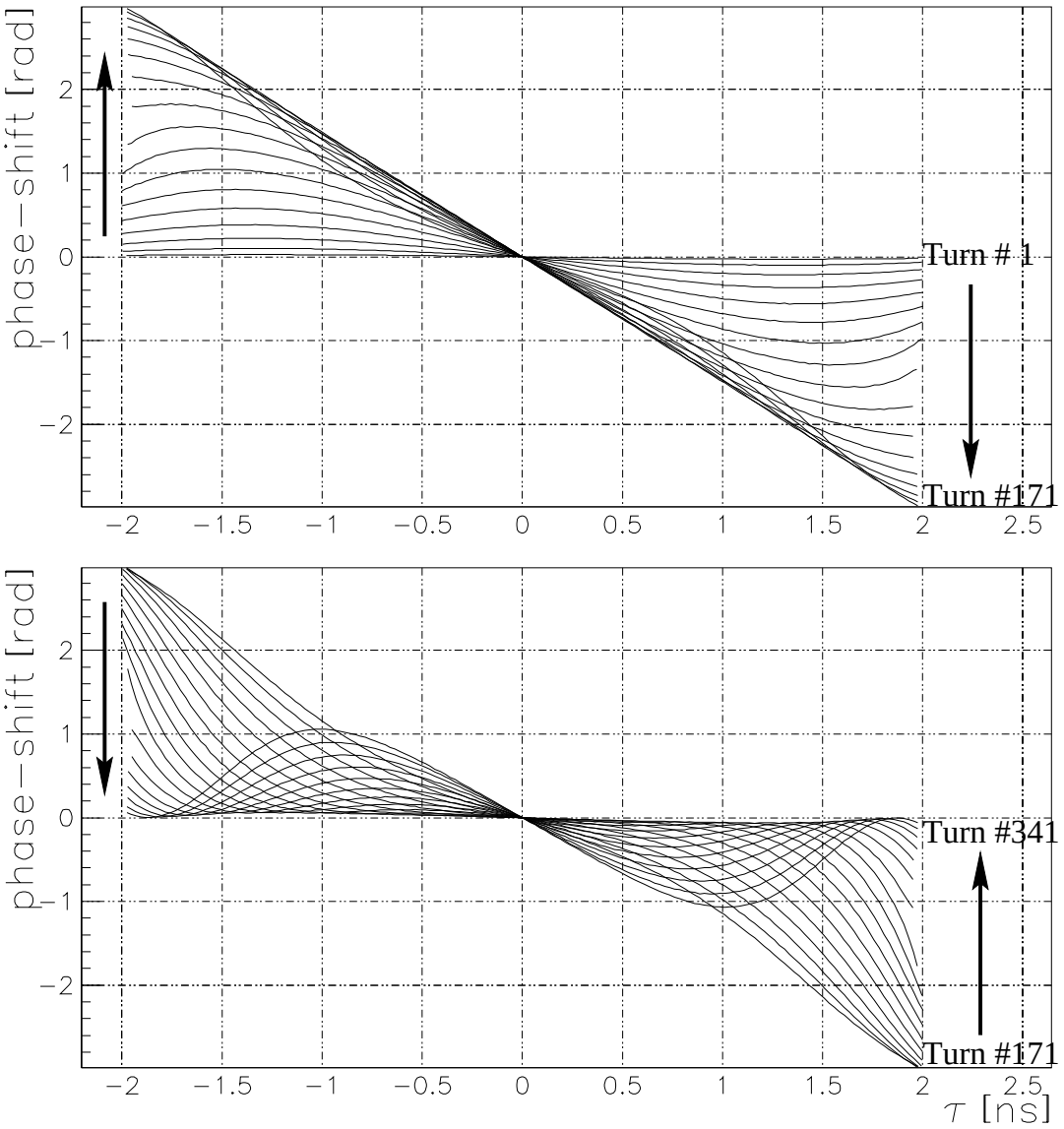

Figure 3: SPS stationary bucket at 265 GeV. Linear chromaticity of 5.1 units. Betatron phase shift $\phi_\beta(\tau; n)$ as a function of τ (see Eq. (22)) tracked over 341 turns after the kick.

3 Explanation and correction of the “Missing Factor” found between Head-Tail and conventional chromaticity measurements

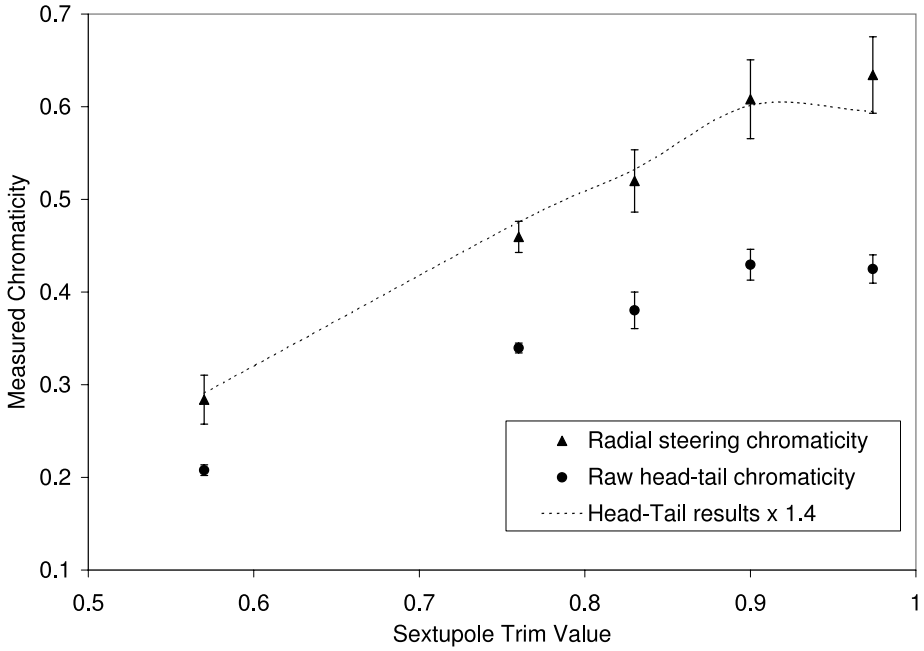

Figure 4: A comparison of head-tail and radial steering chromaticity measured at 303.91 GeV on the CERN-SPS and given in SPS unit ($\xi = Q'/Q = 0.0376 \times Q'$). The head and tail slices are positioned symmetrically around the bunch centre and separated by $\Delta\tau = 1$ ns. The dotted line shows the trend of the head-tail data when corrected by a factor of 1.4.

The head-tail monitor has been operational in the SPS for the last 2 years. A complete description of the detection and acquisition system can be found in [4]. All the results to date have shown discrepancies between the value of chromaticity measured via head-tail phase shifts and the traditional technique of tune tracking during energy modulation (referred to in the SPS as radial steering chromaticity measurements). A typical plot from such a comparison performed at the SPS is shown in Fig. 4, where the measured chromaticity obtained via both the head-tail and radial steering techniques is plot against the sextupole trim. The head-tail data is taken from slices that are symmetrically positioned around the centre of the bunch and separated by $\Delta\tau = 1$ ns. It can be seen that the head-tail results are consistently lower than the actual value, requiring a correction factor of 1.4, which remains essentially constant with chromaticity. The dotted line shows the trend of the head-tail measurements when corrected for this error, which is now seen to be in very good agreement with that measured using energy modulation.
In order to understand the origin of this correction factor, a more detailed study of both the underlying physics of the head-tail phase shift and the acquisition hardware associated with the head-tail monitor was initiated, and is the basis of this paper. From Section 2 it is possible to conclude that for symmetrically positioned head and tail slices there is very little error introduced when considering the two-particle model as opposed to a multi-particle model including non-linearities in the synchrotron motion. This will also be shown to be the case for an accelerating bucket (see Section 4) where further bunch deformations are introduced. With this knowledge, the original simplification in the description of the head-tail phase shift using a simple two-particle model could be excluded as the source of the missing factor. The explanation for this factor was therefore probably associated with the head-tail monitor acquisition chain, and in particular with the effects of bandwidth limitations within the system. A schematic

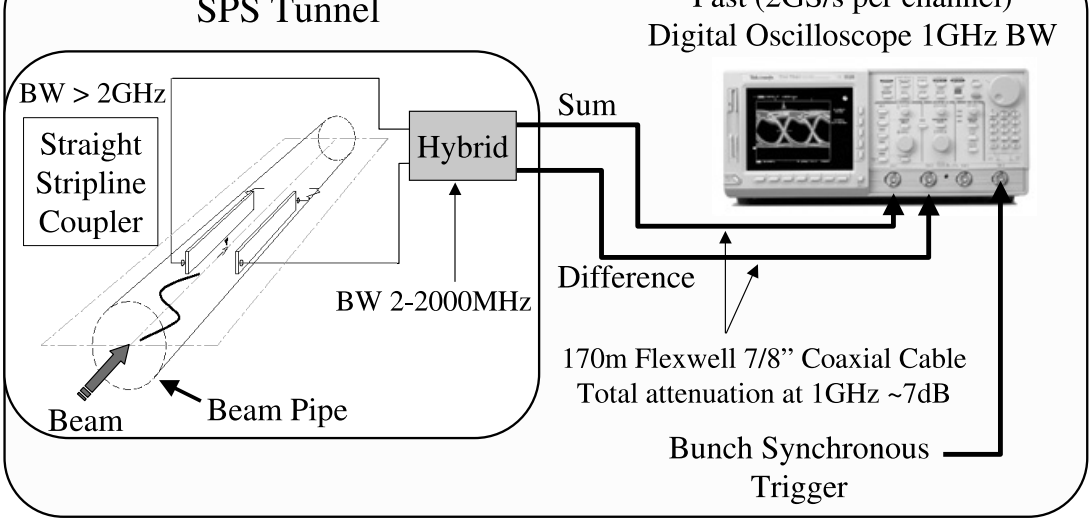

Figure 5: Schematic layout of the head-tail monitor in the CERN-SPS showing the various bandwidth limitations.

layout of the system showing the various bandwidth limitations is shown in Fig. 5.

The main analogue bandwidth limitation within the system comes from the 170 m long cables connecting the hybrid in the SPS tunnel with the acquisition electronics. In addition, the 2 GS/s sampling rate of the oscilloscope reduces the upper frequencies that can be resolved without aliasing after digitisation to around 500 MHz. To see the effect that such bandwidth limitations have on the head-tail measurements, simulations were performed using the turn-by-turn tracking data produced by the beam simulator described in Section 2. The bunch was split into 100 slices to produce both the sum signal (intensity of each slice) and delta signal (position of each slice) for each turn over one synchrotron period. This data was then passed through a PSpice simulation of the coupler and cable (courtesy of D. Cocq) to give a final result that could be interpreted by the head-tail acquisition software. PSpice output files were produced with both 500 ps and 125 ps time intervals between samples, corresponding to 2 GS/s and 8 GS/s sampling rates respectively.

The cable simulation was performed on 3 sets of input data with chromaticities of 1.7, 3.4 and 5.1 units. The resulting output files were passed through the head-tail analysis program. In each case the measured chromaticity was found to be lower than the known chromaticity of the original simulation, requiring a correction factor of ~ 1.3. This was close to the factor of 1.4 found in the real SPS data, and pointed to the cable bandwidth limitations as the main reason for the "missing factor". A simulated delta signal where the head and tail are oscillating out of phase is shown in Fig. 6(a). Also plotted is the resulting signal after having passed through the coupler and cable for both 2 GS/s and 8 GS/s digitisation rates. The effect of the limitations in the bandwidth is clearly shown as an elongation of the original signal (the second, inverted pulse comes from the reflection due to the coupler pick-up).

On the basis of this evidence a deconvolution routine was added to the head-tail analysis program (courtesy of N. Catalan-Lasheras) to take into account the attenuation and phase variations due to the cable. Fig. 6(b) shows the result of deconvolving the output signals shown in Fig. 6(a) with the known simulated cable response. For a sufficiently high sampling rate (8 GS/s in this case) it can be seen that the original signal is perfectly reproduced, as would be expected. The effect of this deconvolution and the sampling rate on the measured value of the head-tail chromaticity is summarised in Table 2. It can be seen that the correction factor is significantly reduced by a deconvolution after 2 GS/s digitisation, and eliminated by a deconvolution after 8 GS/s digitisation.

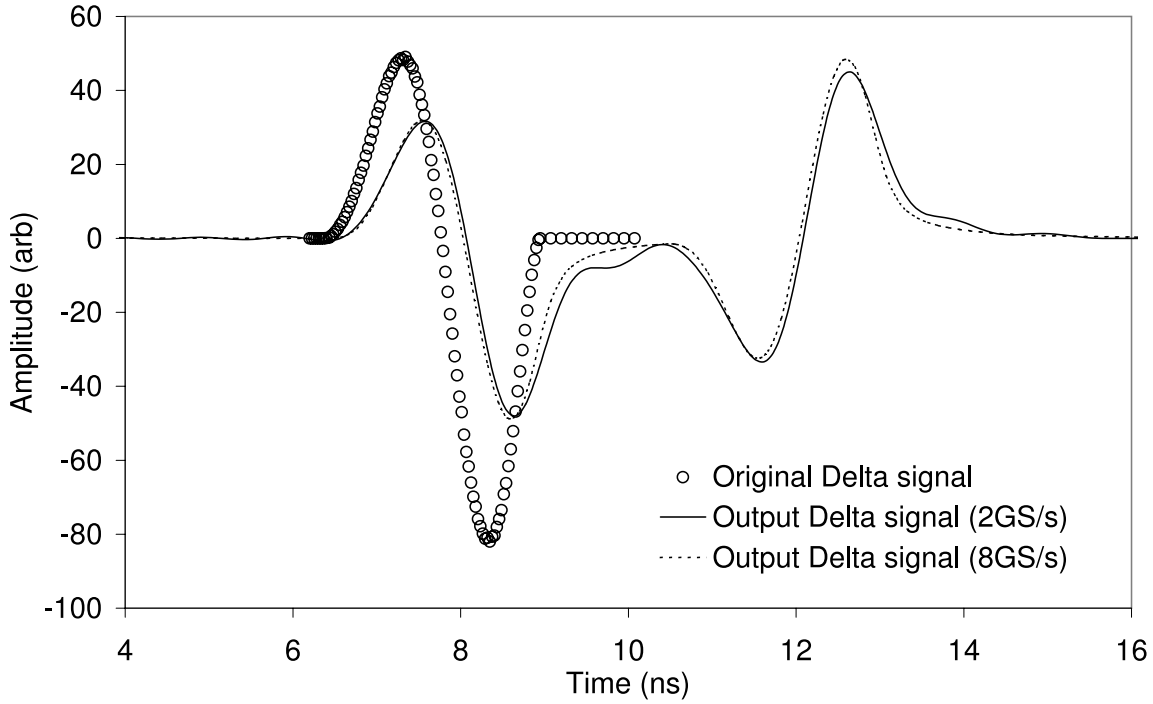

Fig. (a)

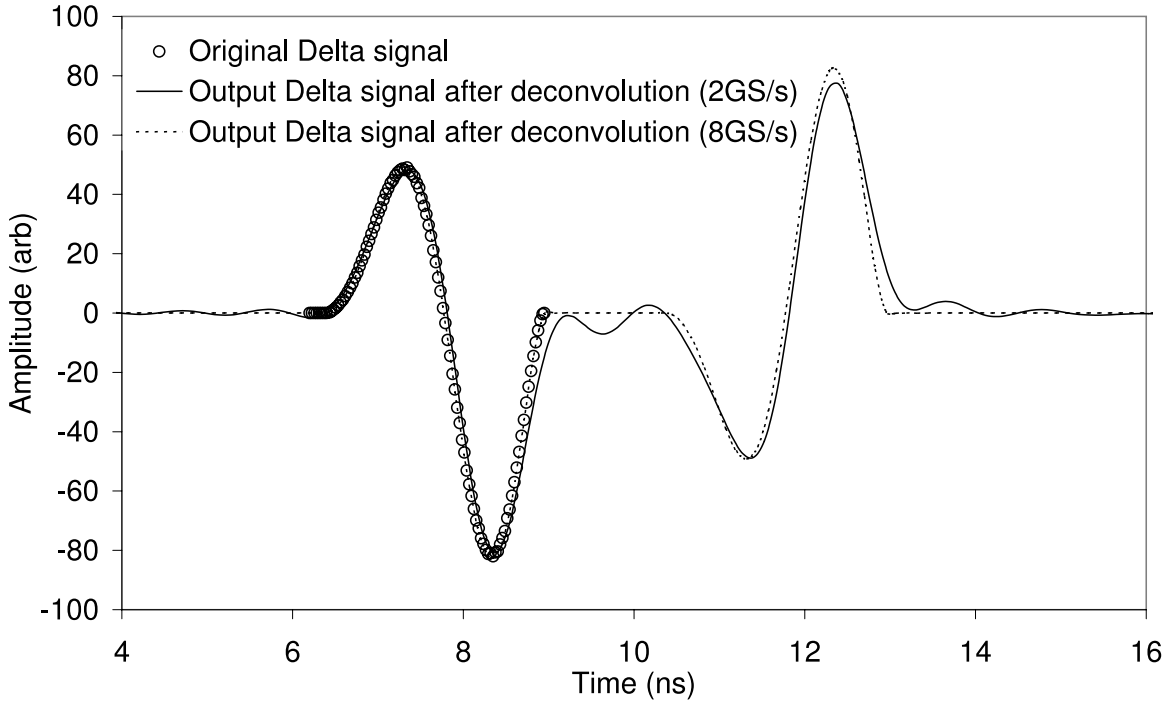

Fig. (b)

Figure 6: The effect of cable bandwidth and sampling rate on an input delta signal (Fig. (a)) and the result of deconvolving the output signal with a known cable response for two different sampling rates (Fig. (b)).

	Required head-tail correction factor		
Chromaticity	No deconvolution	Deconvolution (2 GS/s)	Deconvolution (8 GS/s)
1.7	1.31	1.03	1.00
3.4	1.30	1.03	1.00
5.1	1.29	1.03	1.00
Average	1.30	1.03	1.00

Table 2: The effect of deconvolution (with the simulated cable response) on the head-tail correction factor obtained using simulated data for different values of chromaticity and for different sampling rates.

In order to apply such deconvolution to the measured SPS data the real cable response (amplitude and phase) was required. This was measured in-situ using a network analyser for all frequencies up to 4 GHz (see Fig. 7). Fig. 8 shows the effect of correcting this cable response on the measured value of head-tail chromaticity. In agreement with the simulations, applying this deconvolution significantly reduces the correction factor. A further small correction is obtained if the analogue bandwidth of the oscilloscope is also taken into account, reducing the required correction factor from ~ 1.4 to 1.07-1.11 for chromaticities from 8 to 14 units. For higher chromaticities the effect of deconvolving the 2GS/s digitised data is less pronounced. This is possibly due to the increase in the higher frequency components of the original delta signal which cannot be detected due to the limited sampling rate. The large error bars in the original correction factors come directly from the uncertainty in the measurement of chromaticity via radial steering, with which the head-tail measurements are compared.

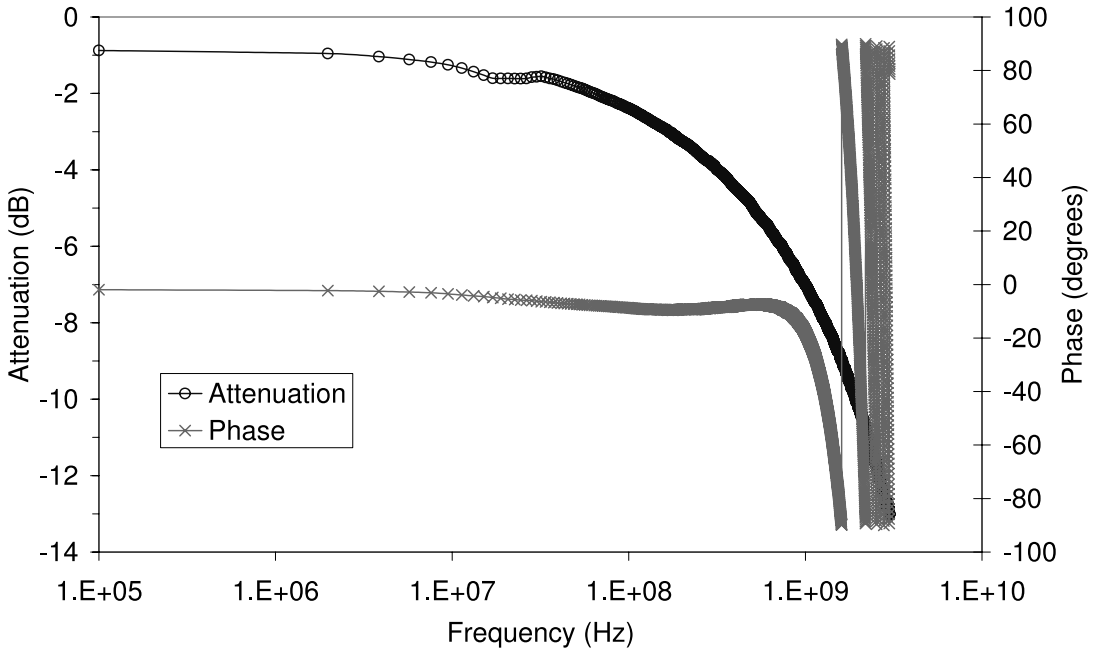

Figure 7: Amplitude and phase response of the 170 m long Flexwell 7/8” cables installed in the SPS between the head-tail monitor pick-up and the acquisition electronics.

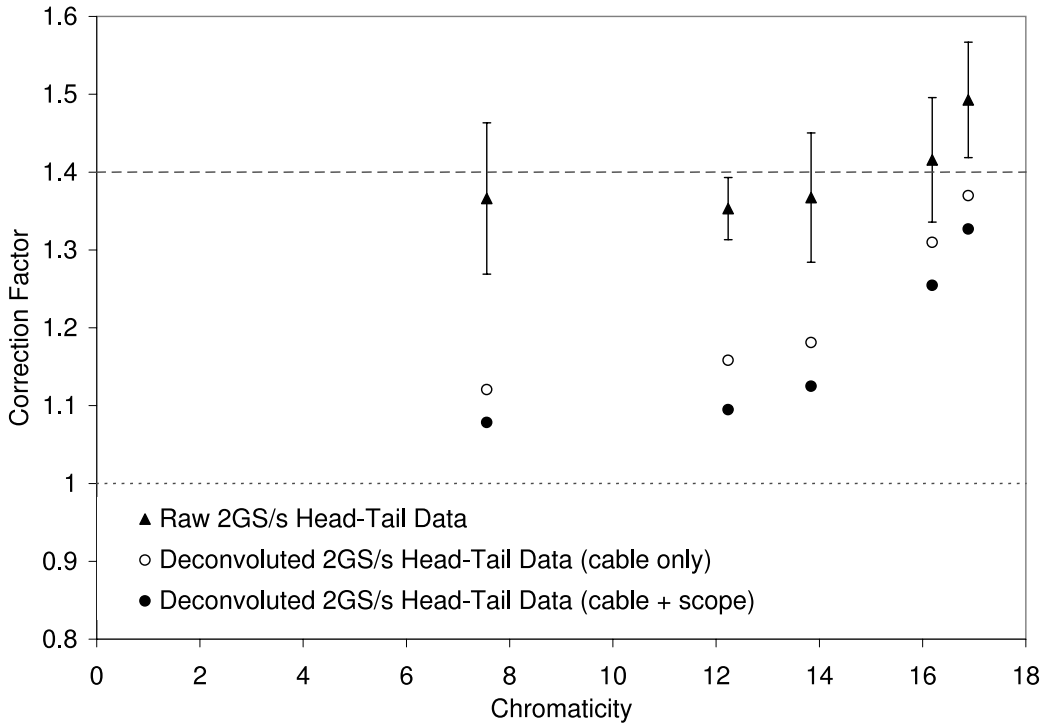

Figure 8: The effect of deconvolution (with the measured cable response) on the head-tail correction factor obtained using measured SPS data for different values of chromaticity.

In all probability the acquisition is now limited by the 2 GS/s sampling rate of the oscilloscope, which effectively reduces the overall bandwidth of the system to around 500 MHz. From the simulations it can be seen that any further improvements to the acquisition chain will therefore require the installation of an oscilloscope capable of sampling at around 8 GS/s.

4 Effect of bunch deformation due to acceleration

When accelerated, the bucket is no longer symmetrical with respect to the point $(z=0,\ \delta=0)$ in longitudinal phase space (see Fig. 1(b)) and, contrary to the case of the stationary bucket treated in Paragraph 2.2.2, the measurement method must be carefully defined.
Results of simulations are shown in the next sub-section for an accelerating SPS bucket at 303.91 GeV. A qualitative explanation of the results obtained follows in Sub-section 4.2, and the experimental verification of the theory will be presented in Sub-section 4.3.

4.1 Results of tracking

The results of tracking obtained for an accelerating SPS bucket at 303.91 GeV are shown in Fig. 9, assuming the RF parameters given in Table 1 and a purely linear chromaticity of 5.1 units (as in Paragraph 2.2.2). Here we have considered the following three cases:

- **case 1.** The two slices used to compute the head-tail phase shift are located at $\tau = \pm 0.5$ ns with respect to the synchronous particle.
- **case 2.** One of the two slices coincides with the bunch centre and the other one corresponds to $\tau = 0.9$ ns (to be compared with $\tau_{\max} = 1.73$ ns in Table 1).
- **case 3.** One of the two slices coincides with the bunch centre and the other one corresponds to $\tau = -0.9$ ns (to be compared with $\tau_{\min} = -1.00$ ns in Table 1).

In the first case (see Fig. 9(a)), analytical estimate (dashed curve) and simulation results (solid line) fit extremely well. As in Paragraph 2.2.2, the only difference lies in a reduction of the

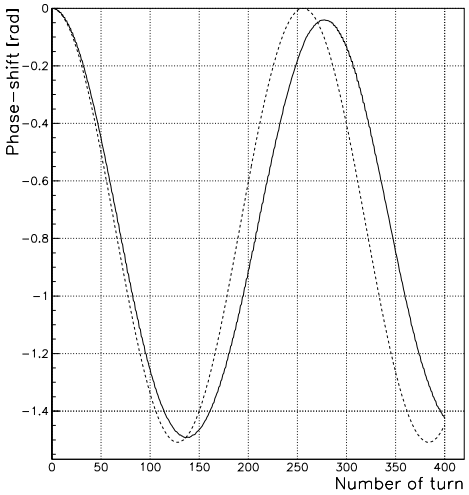

$\longrightarrow$ Betatron phase shift between the slices $\tau = 0.5$ ns and $\tau = -0.5$ ns.

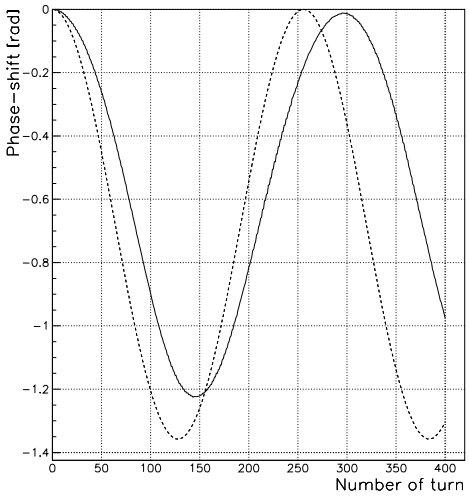

$\longrightarrow$ Betatron phase shift between the slices $\tau = 0.0$ ns and $\tau = 0.9$ ns.

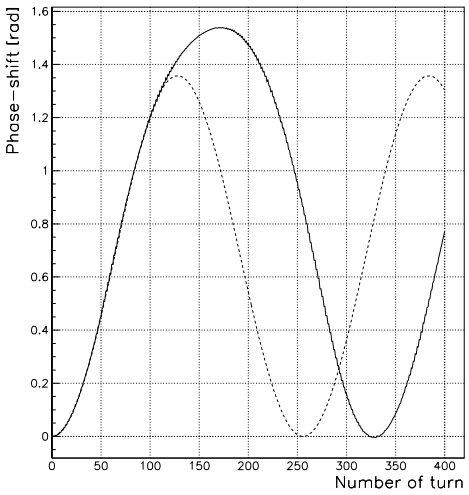

$\longrightarrow$ Betatron phase shift between the slices $\tau = -0.9$ ns and $\tau = 0.0$ ns.

Figure 9: SPS accelerating bucket at 303.91 GeV. Linear chromaticity of 5.1 units. Head-tail phase shift obtained by simulation (solid lines) and comparison with the analytical estimate given in Eq. (8) (dashed curve) for the 3 cases considered in Sub-section 4.1.

modulation frequency of the head-tail phase shift due to the non-linearities of the synchrotron motion. The peak value $\Delta\phi_\beta^{\max}$ attained after the first synchrotron half-period is not affected. As shown in Fig. 9(b), the measurement technique relative to Case number 2 leads to an under-estimate of the chromaticity by some 10%. Conversely the chromaticity can be over-estimated by more than 15% if the measurement is made at the bunch tail and the phase shift computed with respect to the betatron phase of the bunch centre (Case 3). Note also in Fig. 9(c) the significant reduction of the synchrotron frequency when the measurement is made in the vicinity of the tail of the RF bucket.

4.2 Using the two-particle model for a qualitative explanation

As said previously, a fully analytical treatment of the problem has been found extremely difficult, if not impossible in the case of an accelerating bucket. However, as it is often the case, the two-particle model can still be used to give a first estimate of the perturbation induced by acceleration. For this purpose let us consider a single particle with the initial conditions $(z(0) \stackrel{\text{def}}{=} c\tau_0,\ \delta(0) = 0)$ in longitudinal phase space just before the kick. At time $t = s/C$ after the kick, the betatron phase-shift of this particle (w.r.t. the betatron phase of the synchronous particle) is given by

$$\Delta\phi_\beta(s) = \frac{2\pi\, Q'}{C} \int_0^s ds'\ \delta(s')\,, \tag{23}$$

using the notation introduced in Sub-section 2.1. On the other hand, the longitudinal excursion $z(s) \stackrel{\text{def}}{=} c\tau(s)$ of the particle satisfies

$$\frac{dz}{ds} = c\,\frac{d\tau}{ds} = \eta\,\delta(s)\,. \tag{24}$$

As a result, Eq. (23) can also be written as

$$\Delta\phi_\beta(s) = \frac{Q'\,\omega_0}{\eta}\left(\tau(s) - \tau_0\right), \tag{25}$$

which is equivalent to Eq. (3).
To continue the discussion, let us come back to the longitudinal potential $V(\phi)$ given in Eq. (17) and let us introduce the functions $\phi^{\pm}(v)$ defined for the interval $[0, V(\pi - 2\phi_s)]$ and satisfying (see Fig. 10)

$$\phi^+(v) \geq 0\,,\ \phi^-(v) \leq 0 \text{ and } V\left[\phi^{\pm}(v)\right] = v\,, 0 \leq v \leq V(\pi - 2\phi_s)\,, \tag{26}$$

$$\text{giving } \phi^{\pm}\left[V(\phi)\right] = \phi \ \text{ for } \phi \gtrless 0\,. \tag{27}$$

Taking the example of a stationary bucket ($\phi_s = 0$), one has

$$V(\phi) \equiv \sin^2(\phi/2) \Rightarrow \phi^+(v) = -\phi^-(v) = 2\,\sin^{-1}\left(\sqrt{v}\right)\,, 0 \leq v \leq 1\,. \tag{28}$$

Let us assume now that the measurements are taken with a time delay $\tau = \hat{\tau}$ with respect to the bunch centre (slice $\hat{\tau}$). Since the quantity

$$g(z,\delta) \stackrel{\text{def}}{=} \left(\frac{\delta}{\delta_{\max}}\right)^2 + \frac{V(2\pi h z/C)}{V(\pi - 2\phi_s)} \tag{29}$$

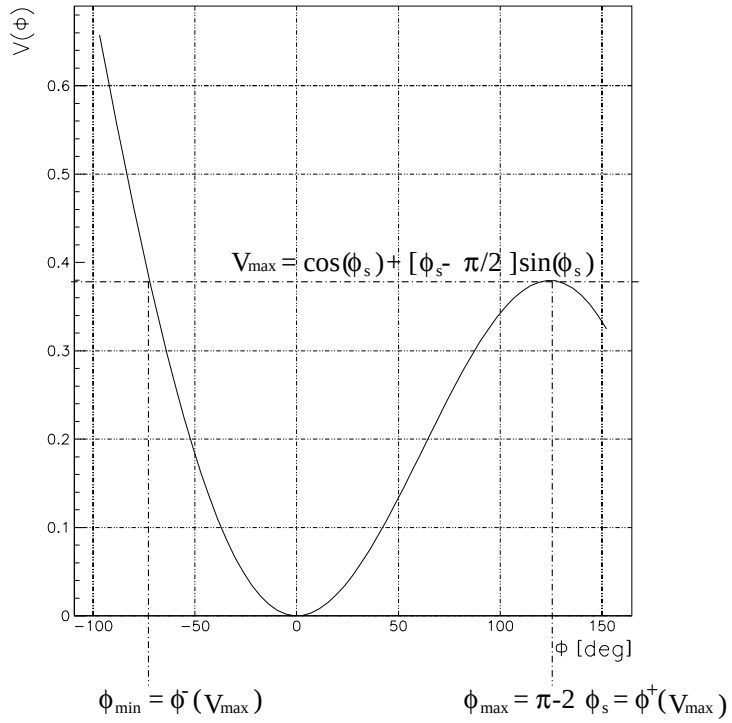

Figure 10: Longitudinal potential $V(\phi)$ defined in Eq.'s (17) assuming a synchronous RF phase of $\phi_s = 27.72°$.

is a constant of motion (see Paragraph 2.2.1), it follows from Eq. (25) that the particle arrives at $\tau(s) = \hat{\tau}$ with a maximum betatron phase shift if its initial condition τ_0 satisfies

$$V(h\,\omega_0\,\tau_0) = V(h\,\omega_0\,\hat{\tau}) \Rightarrow \tau_0 = \frac{1}{h\,\omega_0}\;\phi^{\mp}\left[V(h\,\omega_0\,\hat{\tau})\right],\ \text{whether } \hat{\tau} \gtrless 0. \tag{30}$$

In conclusion, depending on whether the measurement is made at the head ($\hat{\tau} > 0$) or at the tail ($\hat{\tau} < 0$) of the RF bucket, by combining Eq.'s (25) and (30), we obtain

$$\Delta\phi_\beta^{\max}(\hat{\tau}) = S(\hat{\tau})\,\Delta\phi_\beta^{\max,\text{lin.}}(\hat{\tau})\ \text{ with } \begin{cases} \Delta\phi_\beta^{\max,\text{lin.}}(\hat{\tau}) = 2\,\hat{\tau}\,\dfrac{\omega_0 Q'}{\eta} \\ \qquad S(\hat{\tau}) \qquad = \dfrac{\hat{\tau} - \phi^{\mp}\left[V(\omega_{\text{RF}}\hat{\tau})\right]/\omega_{\text{RF}}}{2\,\hat{\tau}}\,, \end{cases} \tag{31}$$

where $\omega_{\text{RF}}/(2\pi)$ denotes the RF frequency. When $\phi_s = 0$ (stationary bucket), it follows from Eq.'s (27) and (28) that $S(\hat{\tau}) = 1$ and Eq. (31) gives an estimate of the head-tail phase shift corresponding to Eq. (9).

The scaling factor $S(\tau)$ is shown in Fig. 11 as a function of τ for different values of the synchronous phase ϕ_s and the 200 MHz RF frequency of the SPS. For $\tau > 0$ (measurement taken at the bunch head) this factor is smaller than unity, which means that Eq. (9), if blindly used, will give an under-estimation of the actual chromaticity. The inverse is true if $\tau < 0$. In fact, from a purely qualitative point of view, this result is evident when looking at the longitudinal phase-space topology of an accelerating bucket[1)] (see Fig 1(b)). For the RF bucket considered in Sub-section 4.1 ($\phi_s = 27.72°$), we find $S(\tau) = 0.9\,/\,1.18$ for $\tau = \pm 0.9$ ns, respectively,

[1)] For a given synchrotron trajectory the ratios $(z_{\max} - z_{\min})/2/z_{\max}$ and $(z_{\min} - z_{\max})/2/z_{\min}$ are smaller and larger than unity, respectively.

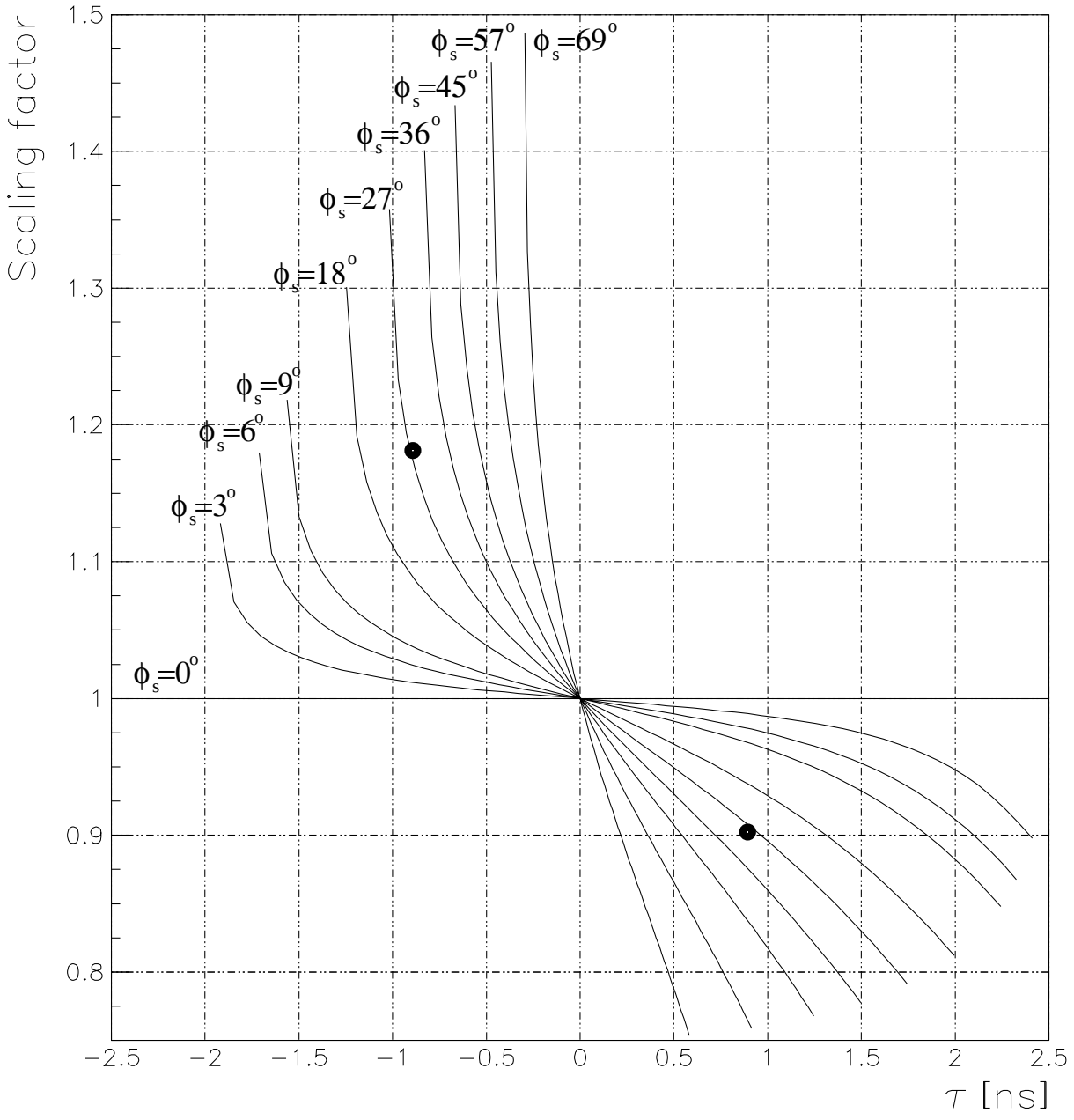

Figure 11: Scaling factor $S(\tau)$ as defined in Eq. (31) for a 200 MHz RF system and different values of the synchronous phase ϕ_s. The bullets refers to Cases 2 and 3 defined in Sub-section 4.1, i.e. $\tau = \pm 0.9$ ns and $\phi_s = 27.72°$.

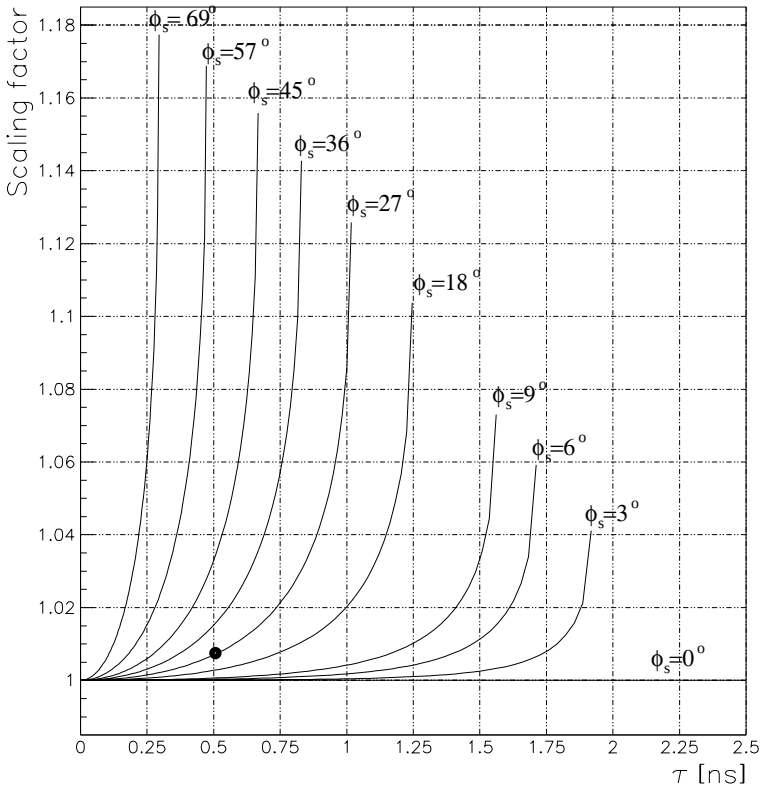

Figure 12: Scaling factor $S_{sym}(\tau)$ as defined in Eq.'s (32) for a 200 MHz RF system and different values of the synchronous phase ϕ_s. The bullet corresponds to $\tau = 0.5$ ns and $\phi_s = 27.72°$.

which matches rather well with the simulation results previously obtained (see Fig.'s 9(b)-(c)). In the case where the betatron phase shift is computed between two slices of charge positioned in a symmetric way with respect to the bunch centre, Eq. (31) must be rewritten by redefining the scaling factor $S(\tau)$ as

$$S_{sym}(\tau) \equiv \big[S(\tau) + S(-\tau)\big]/2\,. \tag{32}$$

For a time separation of 1 ns between the two slices (i.e. $\tau = \pm 0.5$ ns), this factor remains very close to unity (see Fig. 12), which is in agreement with the simulation results shown in Fig. 9(a). Finally, note that this discussion becomes almost irrelevant for an ultra-slow cycling machine such as the LHC where $\phi_s \approx 4° \,/\, 2°$ for the maximum permissible ramp speed of 10 A/s (last segment of the ramp) and a total RF voltage of $V_{\rm RF} = 8 \,/\, 16$ MV.

4.3 Comparison with experiments at the SPS

The effect of bunch deformation due to acceleration on the value of the head-tail chromaticity was investigated in the CERN-SPS during the "25 ns run" with LHC type beam in October 2001. Measurements were performed both during the ramp (accelerating RF bucket) and at high energy (stationary RF bucket) and compared with the simulations and calculations presented in the previous sub-sections. The longitudinal distribution measured for both a stationary and accelerating SPS RF bucket is shown in Fig. 13. These are plotted after correction by deconvolution for the cable between the pick-up and the acquisition electronics (see Section 3) and can be compared to the simulations of Fig. 1. It should be noted that the stationary bucket is reduced in size with respect to that illustrated in Fig. 1 due to the increased energy (450 GeV) at which these measurements took place.

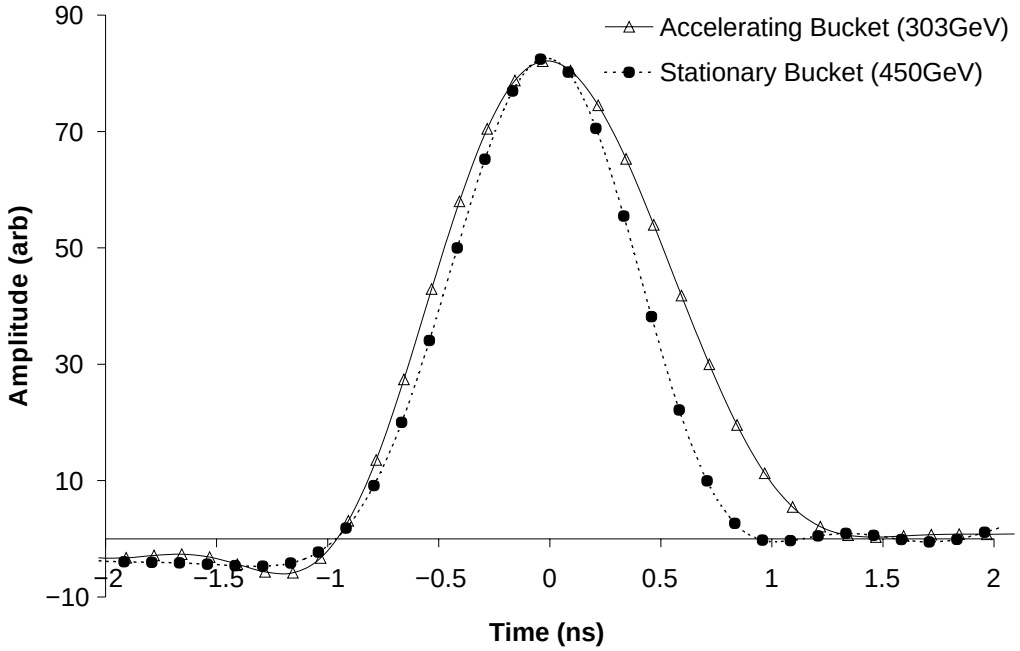

Figure 13: The measured longitudinal bunch distribution after deconvolution for both a stationary and accelerating bucket in the CERN-SPS. The head of the bunch is plotted for positive τ.

The scaling factor $S(\tau)$, as defined in Eq. (31), was measured by comparing the value of the chromaticity at a minimal, symmetric head-tail separation of 0.2 ns ($\tau = \pm 0.1$ ns), with that obtained for a range of asymmetric measurements (see Fig. 14). A positive τ indicates that the measurement took place between the head and centre of the bunch (with the head at time τ from the centre), while a negative τ represents a measurement between the centre and tail of the bunch. In the case of the stationary bucket it can be seen that there is only a slight effect (5-10%) on the value of chromaticity even when the head or tail reach the extreme edges of the distribution, where the effects of non-linear synchrotron motion become important. However, for the accelerating bucket there is a marked difference between measurements taken at the head of the bunch and those taken at the tail. A comparison with the simulations of Fig. 11 show a good agreement in the general trend of the scaling factor, with the measured factor being somewhat larger than predicted.

The symmetric scaling factor $S_{sym}(\tau)$, as defined in Eq. (32), was measured by comparing the value of the chromaticity at a minimal head-tail separation of 0.2 ns ($\tau = \pm 0.1$ ns), with that obtained at larger separations. In each case the head and tail were taken symmetrically about the bunch centre. The results for both the stationary and accelerating bucket are shown in Fig. 15. In the case of the stationary bucket it can be seen that there is little effect on the value of chromaticity until the head-tail separation reaches around 1.2 ns ($\tau = \pm 0.6$ ns), in good agreement with the $\phi_s = 0^\circ$ plot in Fig. 12. Beyond this separation the measurement can overestimate the chromaticity by $\sim 7\%$ for ($\tau = \pm 0.75$ ns). This should not occur for the symmetrical beam distribution of the stationary bucket and is probably due to residual imperfections and noise in the acquisition procedure described in Section 3. For the accelerating bucket the head-tail separation at which the measured chromaticity begins to increase is reduced to around 0.6 ns ($\tau = \pm 0.3$ ns), and can be compared to the trend of the $\phi_s = 27^\circ$ plot in Fig. 12. For a reason which is not clearly understood, the overall scaling factor is found to be significantly larger than that predicted by the simulations.

However, this does not influence the general conclusion of this section, which is that the head-

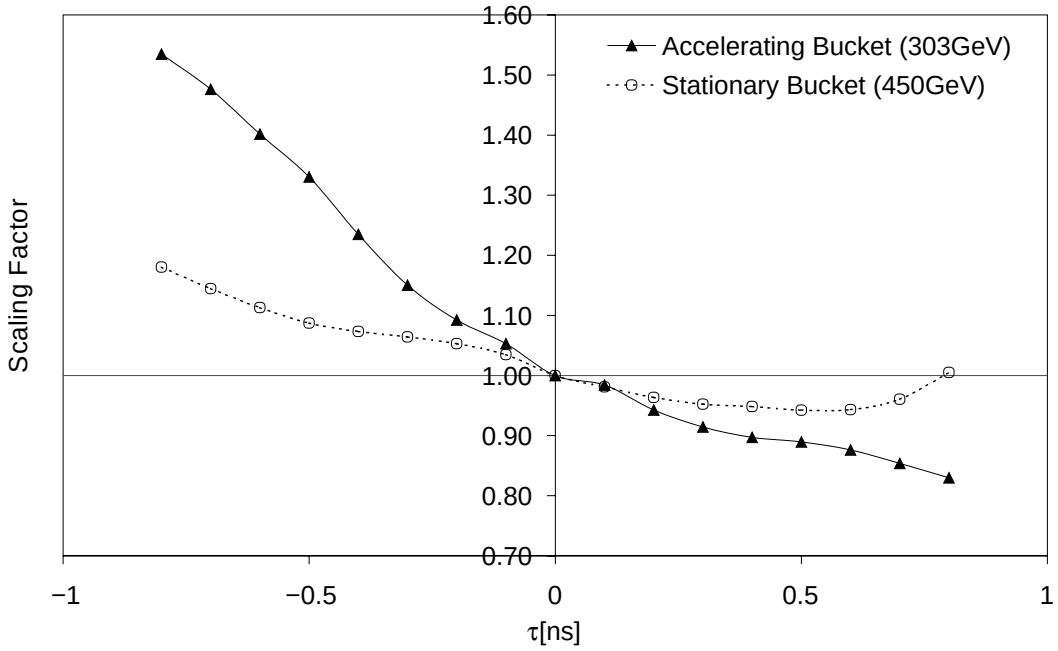

Figure 14: Measured scaling factor $S(\tau)$ (see Eq. (31)) as a function of the head and tail position with respect to the bunch centre. A positive τ represents the head of the bunch with the tail corresponding to the bunch centre, while a negative τ represents the tail of the bunch with the head corresponding to the bunch centre.

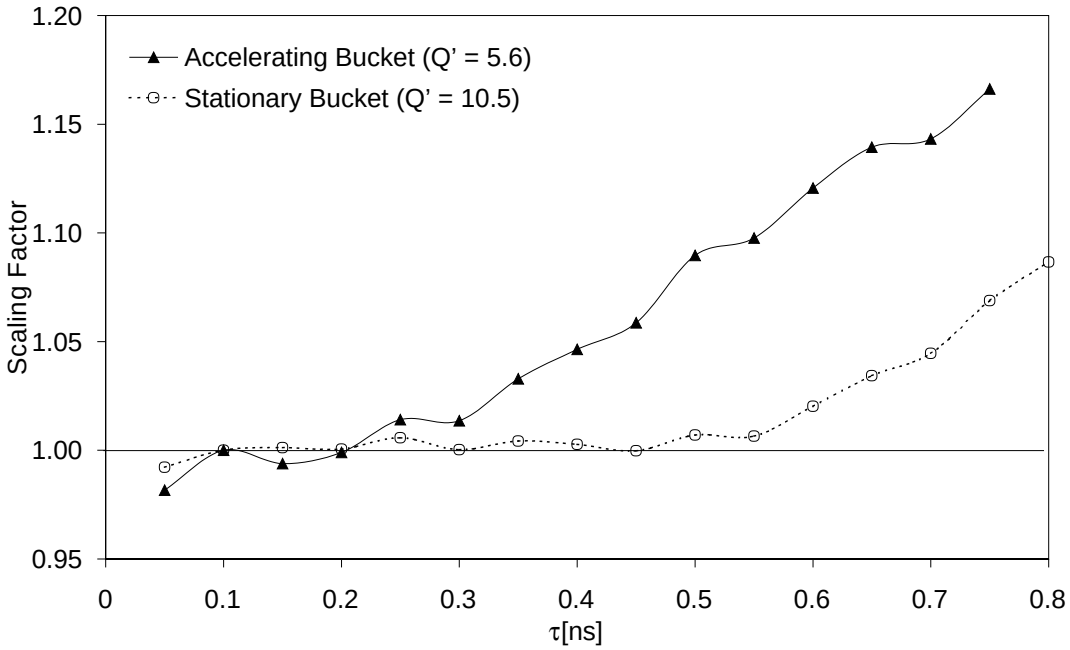

Figure 15: Measured scaling factor $S_{sym}(\tau)$ (see Eq. (32)) as a function of the head and tail position, which are placed symmetrically about the centre of the bunch (i.e. a time separation of 1.0 ns between head and tail is represented by $\tau = 0.5$ ns).

tail chromaticity measurement is valid for both accelerating and stationary RF buckets as long as the measurement takes place symmetrically about the bunch centre using relatively small head-tail separations: in this case up to $\tau = \pm 0.3$ ns for the SPS accelerating bucket and $\tau = \pm 0.6$ ns for the stationary SPS bucket at 450 GeV (and therefore also for the LHC bucket at injection and/or at the beginning of the ramp).

5 Effect of chromatic aberrations

As mentioned in Paragraph 2.2.1, the chromaticity measurement using the head-tail technique is, to a large extent, insensitive to off-momentum β-beating and the presence of spurious dispersion at the monitor. On the other hand, the non-linear chromaticity, if not well controlled during machine operation, can give a non-negligible contribution to the head-tail phase-shift and therefore may deteriorate the accuracy of the monitor. Neglecting the non-linearity of the synchrotron motion and assuming a Gaussian bunch, the contribution of Q'' to the head-tail phase-shift will be estimated analytically in Sub-section 5.1. Results of simulation and analytical estimates will be compared in Sub-section 5.2 in the case of the LHC. In addition, by including the contribution of Q''', it will be shown that the accuracy of the head-tail monitor should not be affected by the non-linear chromaticity expected in the LHC.

5.1 Perturbation induced by Q'': analytical theory in the approximation of a linear synchrotron motion

In order to estimate the contribution of Q'' to the head-tail phase shift, we can follow exactly the same procedure as the one used in Sub-section 2.1, with the exception that the δ-dependence of the betatron tune is now given by

$$Q(\delta) = Q + Q'\,\delta + \frac{1}{2}\,Q''\,\delta^2\,. \tag{33}$$

Assuming the synchrotron motion to be purely linear, a non-synchronous particle undergoes the longitudinal motion given by Eq. (1),

$$\left\{\begin{array}{lcl} z(s;r,\phi_s) & = & r\,\cos\left(2\pi Q_s\,s/C + \phi_s\right) \\ \delta(s;r,\phi_s) & = & -\dfrac{2\pi Q_s}{\eta\,C}\,r\,\sin\left(2\pi Q_s\,s/C + \phi_s\right), \end{array}\right. \tag{34}$$

and, after a transverse kick, will perform betatron oscillations which, turn after turn, can be described by

$$y(n;r,\phi_s) = A\sin\left(2n\pi Q + \theta(n;r,\phi_s)\right)\,, \tag{35}$$

with $\theta(n;r,\phi_s)$ a phase shift given by

$$\theta(n;r,\phi_s) = \frac{2\pi}{C}\int_0^{nC} ds\;\; Q'\times\delta(s;r,\phi_s) + \frac{1}{2}\,Q''\times\delta^2(s;r,\phi_s)\,. \tag{36}$$

The previous integral can be calculated analytically and, as in Sub-section 2.1, the result can be expressed in terms of the actual longitudinal coordinates of the particle, i.e. $c\tau \equiv z(s;r,\phi_s)$ and $\delta \equiv \delta(s;r,\phi_s)$. After some algebra, we get

$$\begin{aligned}\theta(n;r,\phi_s) = {} & \frac{\omega_0\,Q'}{\eta}\,\tau\big(1-\cos(2n\pi Q_s)\big) + \frac{Q'}{Q_s}\,\delta\,\sin(2n\pi Q_s) + \frac{\omega_0\,Q''}{4\eta}\,\tau\delta\,\big(1-\cos(4n\pi Q_s)\big) + \\ & \frac{\pi\,\omega_0^2\,Q_s^2\,Q''}{2\,\eta^2}\,\tau^2\left[n - \frac{\sin(4n\pi Q_s)}{4\pi Q_s}\right] + \frac{\pi\,Q''}{2}\,\delta^2\left[n + \frac{\sin(4n\pi Q_s)}{4\pi Q_s}\right]\,.\end{aligned} \tag{37}$$

Note that the contribution of Q'' contains both a component oscillating at twice the synchrotron frequency and a component increasing linearly with the number of turns. The latter could have been directly deduced from the following observation. Starting from Eq. (33), unlike Q', the second order chromaticity Q'' gives a non-zero contribution to the betatron tune when averaged over a large number of turns. Using Eq. (34), this tune shift can be written as

$$\Delta Q = \frac{1}{2}\,Q''\,\left\langle \delta^2 \right\rangle = \frac{1}{4}\,Q''\,\left(\frac{2\pi Q_s}{\eta C}\right)^2\,r^2 = \frac{1}{4}\,Q''\,\left[\frac{\omega_0^2\,Q_s^2}{\eta^2}\,\tau^2 + \delta^2\right]\,, \tag{38}$$

and the corresponding "betatron phase shift" after turn n is

$$\phi_\beta = 2\pi\,\Delta Q\,n = \frac{\pi\,Q''}{2}\,\left[\frac{\omega_0^2\,Q_s^2}{\eta^2}\,\tau^2 + \delta^2\right] \times n\,, \tag{39}$$

to be compared with Eq. (37).
Assuming the longitudinal bunch distribution $\rho(\tau,\delta)$ to be Gaussian (see Eq. (10)), by combining Eq.'s (35) and (37) and by integrating the obtained result over δ (with the measure $\rho(\tau,\delta)\,d\delta$), the transverse motion of the slice of abscissa τ can be described turn-by-turn by the following expression:

$$\langle y\rangle\,(\tau;n) = A\,(\tau;n)\,\sin\left(2\pi Q\,n + \phi_\beta\,(\tau;n)\right)$$

$$\text{with}\quad \left\{\begin{array}{rcl} A\,(\tau;n) & = & \dfrac{\exp\left(-\dfrac{\tau^2}{2\sigma_\tau^2}\right)}{\sqrt{2\pi}\,\sigma_\tau}\;\dfrac{\exp\left(-\dfrac{\alpha^2(\tau;n)/2}{1+\theta^2(n)}\right)}{\left[1+\theta^2(n)\right]^{1/4}} \\[2ex] \phi_\beta\,(\tau;n) & = & \dfrac{\omega_0\,Q'}{\eta}\,\tau\big(1-\cos(2n\pi Q_s)\big) + \dfrac{\pi\,\omega_0^2\,Q_s^2\,Q''}{2\,\eta^2}\,\tau^2\,\left(n - \dfrac{\sin(4n\pi Q_s)}{4\pi Q_s}\right) - \\ & & \left[\dfrac{\alpha^2(\tau;n)\,\theta(n)}{1+\theta^2(n)} - \arctan\big(\theta(n)\big)\right]/2 \\[2ex] \alpha(\tau;n) & = & \left[\dfrac{Q'}{Q_s}\,\sin(2n\pi Q_s) + \dfrac{\omega_0\,Q''}{4\eta}\,\tau\,\big(1-\cos(4n\pi Q_s)\big)\right]\,\sigma_\delta \\[2ex] \theta(n) & = & \pi\,Q''\,\sigma_\delta^2\left[n + \dfrac{\sin(4n\pi Q_s)}{4\pi Q_s}\right]\;\text{and}\;\;\sigma_\delta = \dfrac{\omega_0\,Q_s}{|\eta|}\,\sigma_\tau\,. \end{array}\right. \tag{40}$$

For $Q'' = 0$, the previous relations reproduce exactly Eq.'s (8) and (11) both for the betatron phase shift $\phi_\beta(\tau;n)$ and for the evolution of the signal envelope $A(\tau;n)$ in the presence of a purely linear chromaticity. On the other hand, for a non vanishing second order chromaticity, the signal decoheres due to the linear increase with n of the angle $\theta(n)$. For instance, the amplitude $A(\tau;n)$ is reduced by a factor of 2 after $n \equiv N_{\frac{1}{2}}$ turns with

$$\theta\left(N_{\frac{1}{2}}\right) = \sqrt{15} \Rightarrow N_{\frac{1}{2}} = \frac{\sqrt{15}}{\pi\,Q''\,\sigma_\delta^2} \sim 500\,\text{turns}\,, \tag{41}$$

for an energy spread σ_δ of 5×10^{-4} (i.e. comparable to the LHC beam energy spread at 450 GeV) and a second order chromaticity as large as 10'000 units (i.e. 10 times higher than its specification given at injection and based on other considerations [5, p. 13]). However, note that

Eq. (41) does not contain the contribution which comes from the betatron non-linearities and which generally dominates. For instance, in the presence of octupolar fields, both the amplitude detuning and the induced second order chromaticity contribute to the decoherence time of the signal but this topics is outside the scope of this paper.
Concerning the betatron phase shift $\phi_\beta(\tau;n)$, Eq. (40) exhibits three main components:

- the first one, proportional to τ, contains the contribution of Q' estimated previously in Eq. (8).
- the second one, proportional to τ^2, was already present in Eq. (37) when describing the effect of Q'' on the betatron motion of a single particle. However this contribution to the head-tail phase-shift can be ignored if the measurements are made for two slices symmetrically positioned with respect to the bucket centre (if one neglects the deformation due to bucket acceleration).
- the third component is the result of the beam filamentation due to Q'' (a multi-particle effect) and is still present in the configuration of two slices symmetrically positioned with respect to the bucket centre. In this configuration, the head-tail phase shift between the two slices can be factorised as

$$\Delta\phi_\beta^{sym}(\tau;n) \equiv \phi_\beta(\tau;n) - \phi_\beta(-\tau;n) = 2\,\tau\,\frac{\omega_0\,Q'}{\eta}\left(1-\cos(2n\pi Q_s)\right)\left(1+\epsilon(n)\right), \tag{42}$$

$$\text{with } \epsilon(n) = -\frac{Q_s\,\omega_0^2\,\sigma_\tau^2}{\eta^2} \times \frac{\theta(n)}{1+\theta^2(n)} \times \cos^2(\pi n Q_s)\,\sin(2\pi n Q_s) \times Q'', \tag{43}$$

and the angle $\theta(n) \propto Q''$ defined in Eq. (40). It is remarkable to see that Eq.'s (8) and (43) have practically the same form; the only difference lies in the "turn-dependent" calibration factor $1+\epsilon(n)$. However, note that this result has been obtained in the approximation of a purely linear synchrotron motion and is valid only in the case where the head-tail phase shift is computed between two slices positioned symmetrically with respect to the centre of the bucket.

5.2 Application to the LHC and simulation in the presence of both second and third order chromaticity

The function $1+\epsilon(n)$ given in Eq. (43) is shown in Fig. 16 taking the LHC beam parameters (see Table 3) and assuming a second order chromaticicity of 10'000 units and 50'000 units at injection and at top energy respectively. At injection, such a second order chromaticity corresponds to an average *uncorrected* b_4 of approximately one unit in the main dipoles, (see [5, Table 22]), that is 3 times more than the value given in the error table 9901. At top energy, the main contribution of Q'' comes from the LHC inner triplets: for the squeezed optics, a second order chromaticity of 50'000 units can only be reached in the case where ATLAS and CMS operate with a β^* of 25 cm (ultimate configuration for protons). On the other hand, Q'' can ideally be set to zero by using the four lattice sextupole families foreseen for the LHC (see [9, Table 2 & 4]). However, in spite of these pessimistic assumptions, the perturbation induced on the measurement of the head-tail phase-shift does not exceed 10-15 % in Fig. 16. Note also that the magnitude of this perturbation remains proportional to Q''^2 (see Eq. (42)), provided that the head-tail phase shift is computed between two slices symmetrically positioned with respect to the bunch centre.
As shown in Fig. 17, this analytical approach allows a full understanding of the evolution of the

Parameter	Symbol	Units	Value	
Ring Circumference	C	m	26658.883	
Harmonic number	h	[1]	$35640\ (400\,\mathrm{MHz})$	
Momentum compaction	α	$[10^{-3}]$	0.347	
Energy	E_s	[GeV]	450	7000
Relativistic factor	γ	[1]	479.605	7460.521
Slippage factor	η	$[10^{-3}]$	-0.343	-0.347
Peak RF Voltage	V_{RF}	[MV]	8.0	16.0
Synchrotron tune (at zero synchrotron amplitude)	Q_s	[turns]	170	472
Bucket half-height	$\delta_{\max}$	$[10^{-3}]$	1.00	0.36
r.m.s. bunch length	σ_τ	[ns]	0.434	0.257
r.m.s. energy spread	σ_δ	$[10^{-3}]$	0.468	0.111

Table 3: Parameters relevant to the LHC RF system, RF voltage and bucket description at injection and top energy [8, p. 167].

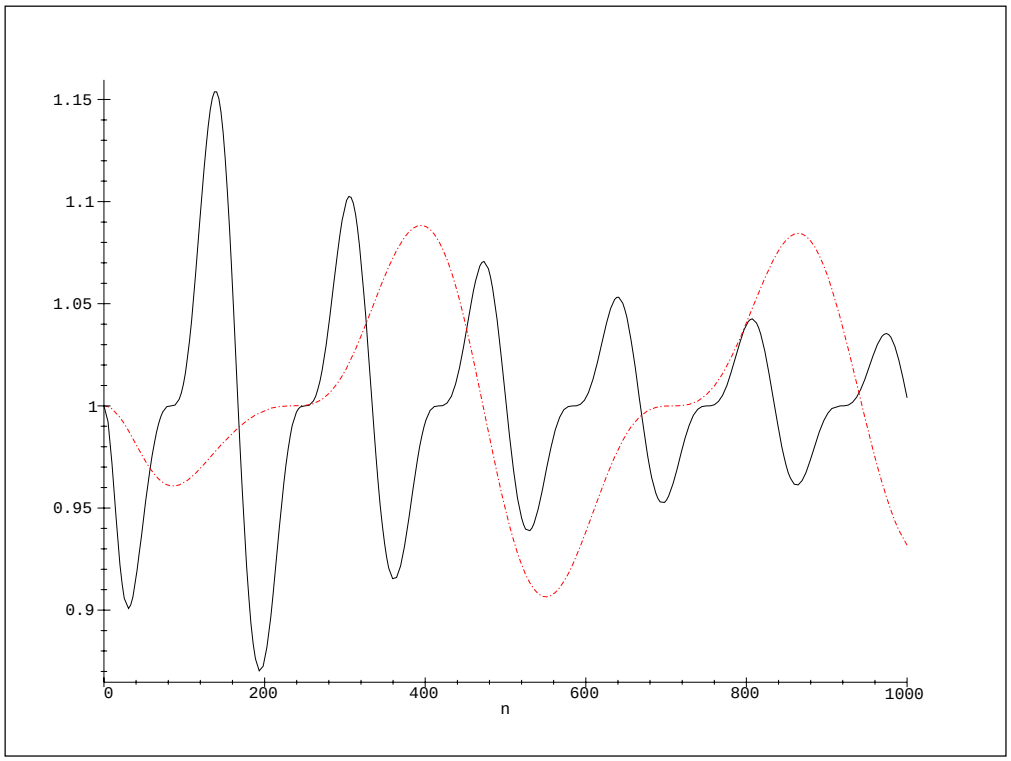

Figure 16: Perturbation due to Q'' in the measurement of the head-tail phase shift between two slices symmetrically positioned around the bucket centre. Calibration factor $1 + \epsilon(n)$ (see Eq.'s (42) and (43)) as a function of the turn number n for the LHC beam parameters, assuming $Q'' = 10'000$ units at injection (solid line) and $Q'' = 50'000$ units at top energy (dot-dashed line).

head-tail phase-shift obtained by tracking for the LHC. When the head-tail phase shift is computed between two slices symmetrically positioned with respect to the bunch centre (Fig.'s 17(a) and 17(c)), the perturbation induced by Q'' is small. In this case and as in Paragraph 2.2.2, the main difference between the tracking results (solid lines) and the analytical estimate derived in Eq. (8) (dashed lines) lies in a reduction of the modulation frequency of the head-tail phase shift. This effect is only related to the non-linearities of the synchrotron motion; the peak value $\Delta\phi_\beta^{\max}$ attained after the first synchrotron half-period is not affected to within a few percent.
In the case where one of the two slices corresponds to the centre of the bucket and the other is located at the head of the bunch (see Fig.'s 17(b) and 17(d)), the contribution of Q'' to the head-tail phase shift is dominant and translates as follows:

- a continuous drift of the head-tail phase-shift. This drift corresponds to the term proportional to $Q''\tau^2$ contained in the expression describing $\phi_\beta(\tau; n)$ in Eq. (40).
- a faster increase of the head-tail phase-shift which stops after turn $n \approx 150$ at 450 GeV (Fig. 17(b)) and $n = 500$ at 7 TeV (Fig. 17(d)). This effect corresponds to the contribution of the term $\arctan(\theta(n))$ in Eq. (40), which is a monotonous function of n (increasing or decreasing with n whether $Q'' \gtrless 0$) and which saturates rapidly when $\theta(n) > 1$, i.e. $n > 1/(\pi\, Q''\, \sigma_\delta^2)$.

To conclude this section, the perturbation induced by a non-vanishing third order chromaticity Q''' has been simulated for the LHC beam in the following two cases:

- LHC beam at 450 GeV with $Q' = 1$, $Q'' = 10^4$ and $Q''' = 10^6$. This third order chromaticity corresponds to an *uncorrected* b_5 of 0.2 units in the main dipoles (see [5, Table 23]) or, in other words, to a relative error of 20% in the setting of the decapole spool-piece correctors MCD (knowing that the expected systematic b_5 is around 1 unit).
- LHC beam at 7 TeV with $Q' = 1$, $Q'' = 5 \times 10^4$ and $Q''' = 3.5 \times 10^7$. At top energy, such a large third order chromaticity can only come from the inner triplets (squeezed optics) assuming ATLAS and CMS to operate with $\beta^* = 25$ cm (see [9, Table 2]).

In both cases, the head-tail phase-shift has been computed between two slices symmetrically positioned with respect to the centre of the bucket (with $\tau_{1,2} \sim \pm\sigma_\tau$). As shown in Fig. 18, the perturbation induced by Q''' is rather small and corresponds to an absolute error of less than $\Delta Q' = 0.2$ units in the estimate of Q' via the head-tail technique.

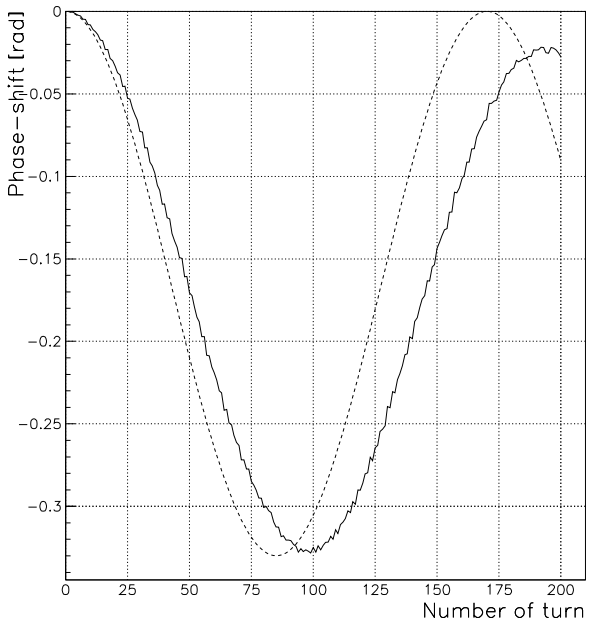

(a): LHC beam 450 GeV, $\tau_{1,2} = \pm 0.4$ ns

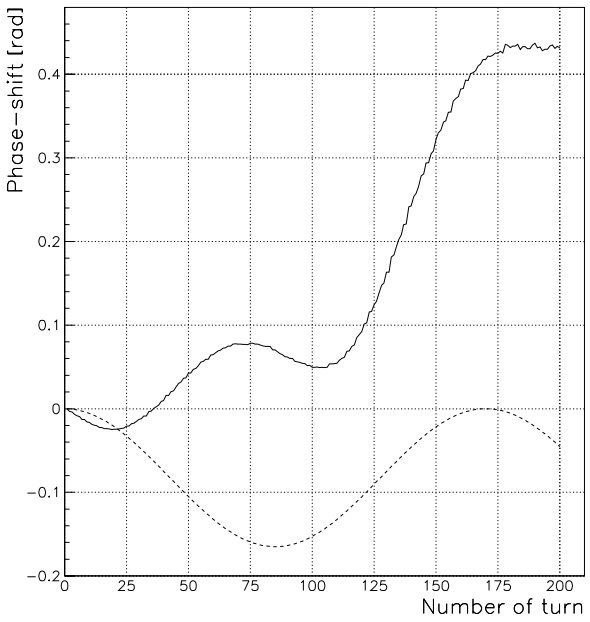

(b): LHC beam 450 GeV, $\tau_1 = 0$ ns, $\tau_2 = 0.4$ ns

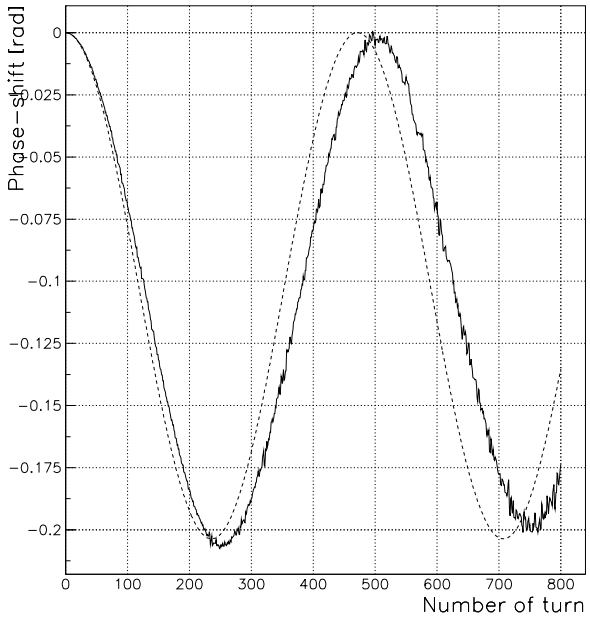

(c): LHC beam 7 TeV, $\tau_{1,2} = \pm 0.25$ ns

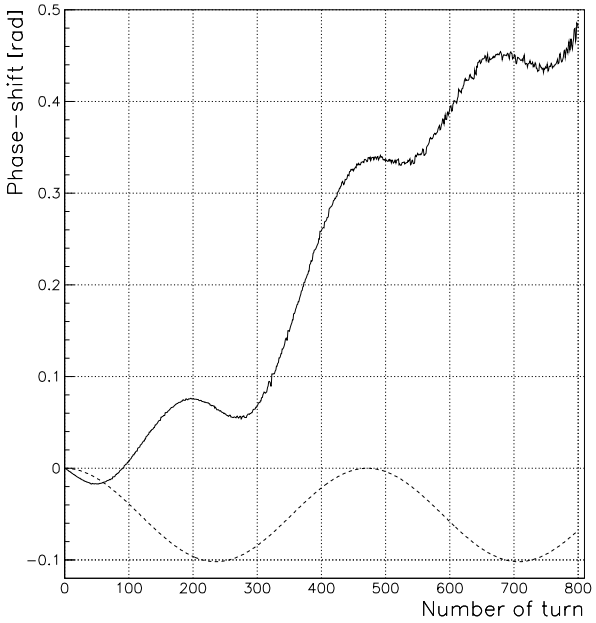

(d): LHC beam 7 TeV, $\tau_1 = 0$ ns, $\tau_2 = 0.5$ ns

Figure 17: Evolution of the head-tail phase shift after a transverse kick in the presence of a non-zero second order chromaticity. Tracking results for the LHC beam (solid lines) assuming a linear chromaticity of 1 unit and a second order chromaticity of 10'000 units at 450 GeV (Fig.'s (a) and (b)) and 50'000 units at 7 TeV (Fig.'s (c) and (d)), and comparison with the analytical estimate given in Eq. (8) (dashed curves). Head-tail phase shift calculated in the following two cases: (1) the two selected slices are symmetrically positioned with respect to the bunch centre at $\tau_{1,2} \approx \pm\sigma_\tau$ (Fig.'s (a) and (c)); (2) the first slice corresponds to the centre of bucket ($\tau_1 = 0$), the other one being located at the bunch head at $\tau_2 \approx \sigma_\tau$ (Fig.'s (b) and (d)).

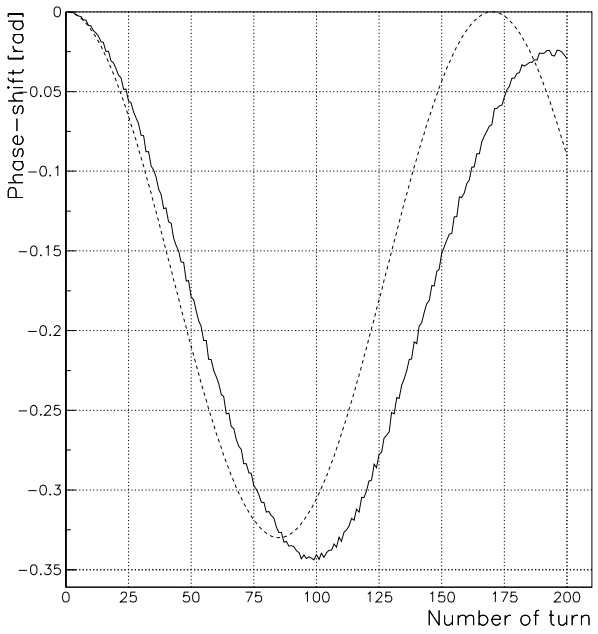

(a): LHC beam 450 GeV, $\tau_{1,2} = \pm 0.4$ ns

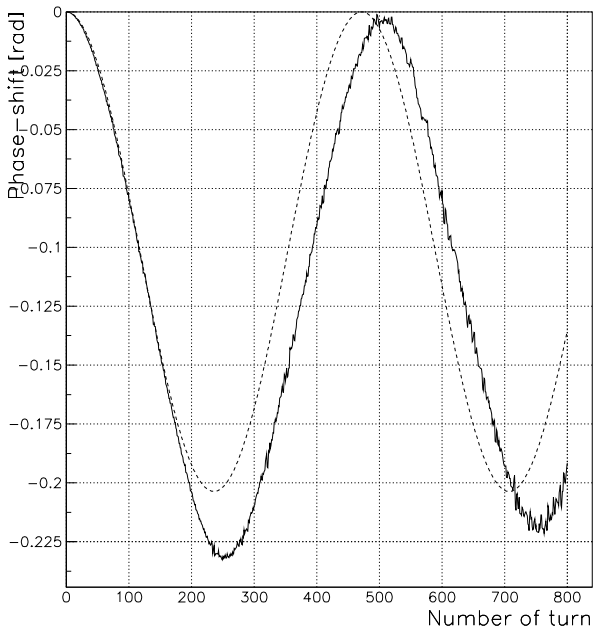

(b): LHC beam 7 TeV, $\tau_{1,2} = \pm 0.25$ ns

Figure 18: Evolution of the head-tail phase shift after a transverse kick in the presence of both a second and third order chromaticity. Tracking results for the LHC beam (solid lines) assuming $Q' = 1$, $Q'' = 10 \times 10^3$ (resp. $Q'' = 50 \times 10^3$) and $Q''' = 10^6$ (resp. $Q'' = 35 \times 10^6$) at 450 GeV (Fig. (a)) and 7 TeV (Fig. (b)) respectively, and comparison with the analytical estimate given in Eq. (8) (dashed curves). Head-tail phase shift calculated between two bunch slices symmetrically positioned with respect to the bunch centre.

6 Other possible perturbations and outstanding issues

Other possible perturbations such as coupling or transverse impedance may also deteriorate a priori the precision of the measurement. However, we will see in the next sub-sections that this should not be the case for the LHC. In fact, the only real limitation to the head-tail technique comes from the transverse excitation scheme which is currently used. Indeed, the transverse resolution of the monitor requires large kicks with amplitudes of the order of 1 mm, which corresponds roughly to $1\ \sigma$ and $4\ \sigma$ in the LHC arcs at 450 GeV and 7 TeV respectively. As a result, during LHC luminosity runs, the use of the head-tail monitor is presently excluded for the following two reasons: to conserve the transverse emittance of the beam and to exclude the possibility that one of the secondary collimators becomes a primary. On the other hand, alternative excitation schemes may be envisaged and will be mentioned in the conclusion of this report.

6.1 Coupling

Let us assume the beam to be excited in the horizontal plane. In the presence of linear coupling between the two transverse planes, the horizontal signal extracted from the head-tail monitor can be decomposed in the basis of the two betatron eigen modes:

$$\langle x \rangle (\tau; n) = A_{x_I} \sin\big(2n\pi Q_I + \phi_{\beta_I}(\tau; n)\big) + A_{x_{II}} \sin\big(2n\pi Q_{II} + \phi_{\beta_{II}}(\tau; n)\big)\,, \qquad (44)$$

with $Q_{I,II}$ the two transverse eigen tunes and $\phi_{\beta_{I,II}}(\tau; n)$ the corresponding betatron phase shifts (given with respect to the slice $\tau = 0$). Written like this, the results obtained in the

un-coupled case can be directly transposed in the present case concerning the contribution of the linear and non-linear chromaticities, $Q'_{I,II}$, $Q''_{I,II}$ ..., to the head-tail phase-shifts $\phi_{\beta_{I,II}}$. Moreover, for a partially coupled machine[2)], the amplitude $A_{x_{II}}$ is proportional to the square of the perturbation (that is the skew quadrupole field errors of the lattice). More precisely, we have

$$A_{x_{II}}/A_{x_I} \propto \tan^2\big(\phi(s_0)\big) \tag{45}$$

where s_0 denotes the longitudinal position of the head-tail monitor in the ring and $\phi(s_0)$ is the angle of the symplectic 4D-rotation which block-diagonalised the transverse one-turn map $R(s_0 \rightarrow s_0+C)$ (Edwards and Teng method [10]). In other words, the angle $\phi(s_0)$ characterises the orientation of the beam ellipse at the location of the monitor. After coupling correction in the LHC (based on an arc-by-arc minimisation of the difference coupling coefficient followed by a global correction using the closest tune approach), the angle $\phi(s)$ does not exceed a few degrees in the machine [11]. As a result, coupling, if carefully controlled, should not interfere with the head-tail technique to measure Q' in the LHC.

6.2 Head-tail phase shift due to transverse impedance in the SPS at low energy and extrapolation to the LHC

Dedicated measurements of the head-tail phase shift were performed at the SPS at 26 GeV for a bunch population ranging from $N=10^{10}$ to $N=8.9\times10^{10}$ particles. During the measurement, the linear chromaticity was carefully adjusted to zero with the usual radial steering technique and the RF voltage was set to its standard value at injection, i.e. 0.8 MV corresponding to a synchrotron period of about $1/Q_s = 283$ turns; the beam was excited in the vertical plane, data were taken for two portions of bunch spaced by $\Delta\tau = 0.5$ ns and the measured r.m.s. bunch length was around $\sigma_\tau = 0.5$ ns. As shown in Fig. 19, for $N = 8.9 \times 10^{10}$, the maximum head-tail phase shift is reached at turn $n \approx 250$ and corresponds to $\Delta\phi_\beta^{\max} = -1.2$ rad.
Starting from this experimental result, the effect expected at 450 GeV in the LHC can be roughly estimated in the following way:

– the betatron coherent tune shift due to short-range transverse wake-fields varies as (see e.g. [13])

$$\Delta Q = \Delta\omega_\beta/\omega_0 \propto \frac{N\,\mathrm{Im}\left[(Z_\perp)_{\text{eff}}\,(\omega_\xi)\right]}{\gamma\,\omega_0\,Q\,\sigma_z}\,, \tag{46}$$

with ω_0 the angular revolution frequency, γ the Lorentz factor, N the number of particles per bunch, σ_z the r.m.s. bunch length, $\omega_\xi = Q'\omega_0/\eta$ the chromatic frequency, $\eta = -0.5158 \times 10^{-3}$ the slippage factor of the SPS at 26 GeV, and $(Z_\perp)_{\text{eff}}\,(\omega)$ the effective transverse impedance at the angular frequency ω given by the convolution product between the total transverse impedance of the ring and the frequency spectrum $h_0(\omega)$ of the longitudinal bunch distribution:

$$(Z_\perp)_{\text{eff}}\,(\omega_\xi) = \int_{-\infty}^{\infty} d\omega Z_1^\perp(\omega)\,h_0(\omega-\omega_\xi)\ . \tag{47}$$

For the year 2001, measurements of single-bunch coherent tune shifts in the SPS [12] gave

$$\mathrm{Im}\left[(Z_y)_{\text{eff}}^{\text{sps}}\right] \lesssim 20\ \mathrm{M\Omega/m} \tag{48}$$

[2)] "Partially coupled machine" means that the modulus of the difference coupling coefficient remains lower than the unperturbed fractional tune split $Q_x - Q_y$.

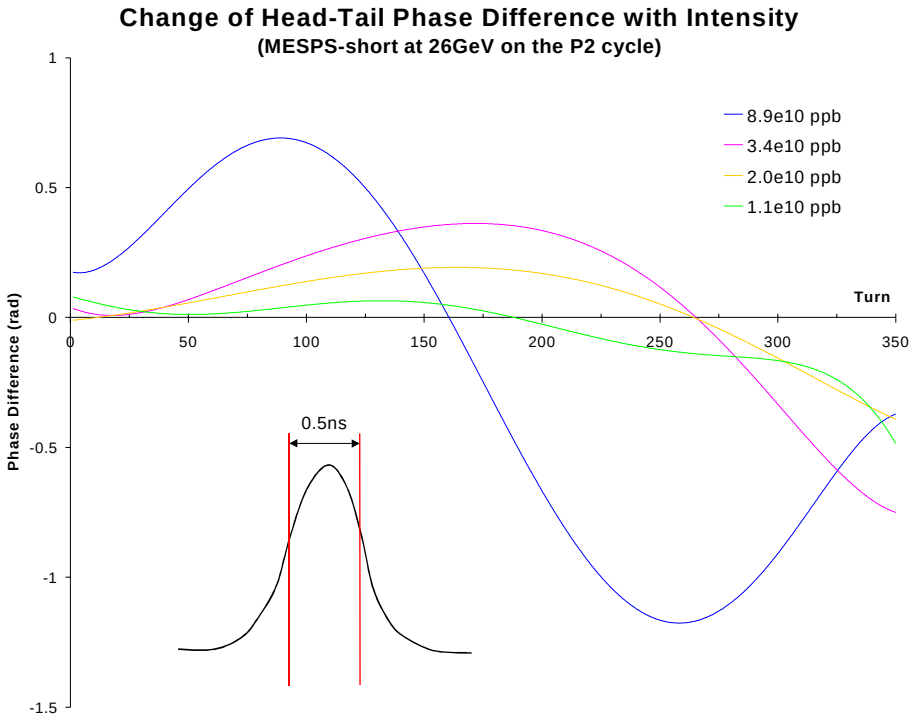

Figure 19: Head-Tail phase difference for zero chromaticity in the presence of transverse impedance. Measurements performed on a single bunch at 26 GeV in the SPS for varying intensities.

for the vertical plane and for low frequencies (i.e. overlapping with the bunch power spectrum $h_0(\omega)$). At those frequencies, the imaginary part of the transverse effective impedance in the LHC has been evaluated to [14]

$$\beta_{\rm av}\,{\rm Im}\left[(Z_\perp)_{\rm eff}\right] \lesssim 629.4\ {\rm M}\Omega,\ \text{giving}\ \ {\rm Im}\left[(Z_\perp)_{\rm eff}\right] \lesssim 8\ {\rm M}\Omega/{\rm m}\,, \tag{49}$$

for an average beta function of $\beta_{\rm av} = 80$ m. Note that an updated review [15] of the LHC impedance budget gives around twice less, i.e. 4 MΩ/m, for the total transverse broadband impedance of the LHC ring. However, this factor of 2 will be kept in the following as a safety margin concerning the possible effects that the transverse impedance of the LHC may have on the accuracy of the head-tail chromaticity measurement technique.

– in the absence of synchrotron motion (i.e. $Q_s = 0$ corresponding to a rigid bunch going trough a linac), a given particle located say at the head of the bunch will be insensitive to the transverse machine impedance (for frequencies larger than the bunch to bunch repetition frequency). In this case, the betatron phase advance of this particle calculated with respect to that of the particles belonging to the core of the bunch will grow linearly turn after turn:

$$\Delta\phi_\beta^{(Q_s=0)} \sim -\Delta Q \times n\,. \tag{50}$$

On the other hand, for $Q_s \neq 0$, the particle considered oscillates at the synchrotron frequency between the head and the tail of the bunch, leading to a modulation of the head-tail phase-shift. The amplitude $\Delta\phi_\beta^{\rm max}$ of this modulation can then be directly deduced from

the previous equality by replacing n with $1/Q_s$:

$$\Delta\phi_\beta^{\max} \sim \Delta Q/Q_s \propto \frac{N\,\mathrm{Im}\left[(Z_\perp)_{\mathrm{eff}}\right]}{\gamma\,\omega_0\,Q\,Q_s\sigma_z}\,. \tag{51}$$

Considering the nominal LHC beam parameters given in Table 3, taking 26 and 60 units for the integer part of the betatron tune in the SPS and in the LHC respectively, and combining Eq.'s (48), (49) and (51), the head-tail phase shift of 1.2 rad peak measured at 26 GeV in the SPS can be extrapolated at 450 GeV for the LHC:

$$\Delta\phi_\beta^{\max} \approx \frac{\overbrace{(1.1/0.89)}^{\text{Scaling of } N} \times \overbrace{(8/20)}^{\text{Scaling of } Z_\perp} \times \overbrace{1.2}^{\Delta\phi_\beta^{\max} \text{ measured in the SPS}}}{\underbrace{(450/26)}_{\text{Scaling of }\gamma} \times \underbrace{(6906.765/26658.883)}_{\text{Scaling of }\omega_0} \times \underbrace{(60/26)}_{\text{Scaling of } Q} \times \underbrace{(300/170)}_{\text{Scaling of } Q_s} \times \underbrace{(0.434/0.5)}_{\text{Scaling of }\sigma_\tau}} \approx 0.04\,\mathrm{rad}\,. \tag{52}$$

As shown in Fig. 17(a), one unit of chromaticity corresponds to a head-tail phase shift of 0.33 rad peak for the LHC at 450 GeV and for two slices spaced by $\Delta\tau = 0.8$ ns (to be compared with the time separation of 0.5 ns considered in Fig. 19). As a result, the perturbation induced by the transverse impedance of the ring and expressed in terms of effective linear chromaticity should not exceed $\Delta Q' \approx 0.04/0.33 \times 0.8/0.5 \approx 0.2$ units at injection, which is rather acceptable. Moreover, note that this estimate stands only for nominal LHC bunches and would become pessimistic in the case where bunches of intermediate intensity would be "sacrificed" (in terms of beam emittance) for chromaticity measurements during luminosity runs.

7 Conclusions

On the experimental side, both the method and acquired data is now much better understood. The addition of the deconvolution routine into the analysis algorithm to take account of cable attenuation has significantly reduced the "missing factor" between the head-tail and traditional chromaticity measurements. Some discrepancy still remains, in particular for high values of chromaticity, which is probably a result of the 2 GS/s limited sampling rate of the oscilloscope.

In agreement with the simulations, it has been experimentally verified that the method is applicable both for stationary and accelerating buckets with the constraint that the measurement is performed close to and symmetrically about the bunch centre. In addition, dedicated calculations performed for the LHC have demonstrated the robustness of the head-tail technique in the presence of off-momentum beta-beating, non-linear chromaticity, Q'' and Q''', or linear coupling (if the latter is arc-by-arc compensated as foreseen in the LHC). Finally, an extrapolation of the SPS data taken at 26 GeV seems to indicate that, at nominal current, the accuracy of the head-tail chromaticity technique should practically not be affected by the transverse impedance of the LHC ring.

For the future, a new system working with sampling rates of up to 10 GS/s will be installed in the SPS. It is hoped that this increase in the sampling rate along with the continued deconvolution of the cable response will completely eliminate the residual "missing factor". In addition, closed orbit compensation electronics will be added to improve the sensitivity of the acquisition, and allow the measurement to be made with much smaller excitation amplitudes. Several alternative excitation schemes will also be investigated, e.g. swept frequency and "so called" AC-dipole excitation [16], which may also allow the use of head-tail phase shift information with, hopefully, a better control of the induced emittance growth.

References

[1] H. Schmickler, “Diagnostics and Control of the Time Evolution of Beam Parameters” (CERN-SL-97-68), presented at the 3rd European Workshop on Beam diagnostics and Instrumentation for Particle Accelerators (DIPAC’97), Frascati, Italy, October 1997.

[2] D. Cocq, O. R. Jones, H. Schmickler, “The Measurement of Chromaticity via a Head-Tail Phase Shift”, 8th Beam Instrumentation Workshop (BIW’98), Stanford, CA, USA, May 1998.

[3] A. Boudsko, O. R. Jones, H. Schmickler, M. Wendt, F. Willeke, “Chromaticity Measurements at Hera-p using the Head-Tail Technique with Chirp Excitation”, proceedings of the 4th European Workshop on Diagnostics and Instrumentation for Particle Accelerators (DIPAC’99), Chester, UK, May 1999.

[4] R. Jones, H. Schmickler, “The measurement of Q' and Q'' in the CERN-SPS by head-tail phase shift analysis” (CERN-SL-2001-020-BI), presented at the IEEE Particle Accelerator Conference, Chicago, IL, USA, 18 - 22 June 2001.

[5] S. Fartoukh, O. Brüning, “Field quality specification for the LHC Main dipole Magnets”, LHC Report 501, October 2001.

[6] E. Shaposhnikova, “Longitudinal stability of the LHC beam in the SPS”, SL-Note-2001-031 HRF, August 2001.

[7] D.J. Sakrison, “Communication Theory: transmission of waveforms and digital information”, Chapter 5, Wiley, N.Y.

[8] The LHC study group, “The Large Hadron Collider, Conceptual design”, CERN/AC/95-05 (LHC), Oct. 1995.

[9] S. Fartoukh, “Second order chromaticity correction of LHC V6.0 at collision”, LHC Project Report 308, Oct. 1999.

[10] L.C. Teng, “Concerning n-Dimensional Coupled Motion”, FN 229, FNAL, 1971.

[11] O. Brüning, “Linear coupling compensation for the LHC Version 6.1”, EPAC 2000, 26-30 June 2000, Vienna and LHC Project Report 399, Aug. 2000.

[12] H. Burkhardt, G. Rumolo, F. Zimmermann, “Measurements of SPS Single-Bunch Coherent Tune Shifts and Head-Tail Growth Rates in the Year 2001”, SL Note 2001-043 (MD), Dec. 2001.

[13] F. Sacherer, “Single-beam collective phenomena, Transverse, Bunched Beams”, Proceedings of the 1976 Erice school on accelerators, M.H. Blewett (Ed.), CERN yellow report 77-13, 1977.

[14] F. Ruggiero, “Single Beam Collective Effects in the LHC”, CERN SL/95-09 (AP), June 1995.

[15] D. Brandt, L. Vos, D. Angal-Kalinin, “Intermediate review of single bunch collective effects in the LHC”, EPAC2002 Proc., Paris, France, 3 - 7 June 2002.

[16] O. Berrig, W. Höfle, R. Jones, J.P. Koutchouk, H. Schmickler, F. Schmidt, “Excitation of Large Transverse Beam Oscillations without Emittance Blow-up using the AC-Dipole Principle” (CERN-SL-2001-019-BI), presented at the 5th European Workshop on Diagnostics and Beam Instrumentation, Grenoble, France, 13 - 15 May 2001.